Nonlinear evolution-II: halo abundances

Halo mass functions at different redshifts. Abundances of dwarfs and satellites.

Abundance of dark matter halos

- Analytics: expectations

- Simulations: LCDM predictions
  - Halos and Subhalos abundances
  - Warm Dark matter vs. LCDM

- Field Galaxies overabundance problem

- Local Group: overabundance problem/ missing satellite problem

The 'tophat model' (spherical collapse)

- consider a uniform, spherical perturbation

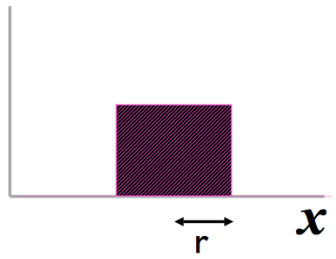

$\delta_i = \rho(t_i)/\rho_b(t_i) - 1$

$M = \rho_b(4\pi r_i^3/3)(1+\delta_i)$

equation of motion for the perturbation (same as for a closed universe)

$$\ddot{r} = -\frac{GM}{r^2}$$

integrating

$$\frac{1}{2}\dot{r}^2 - \frac{GM}{r} = E = \text{constant}$$

at turnaround,

$$E = -\frac{GM}{r_{\max}}$$

the perturbation will be in virial equilibrium when

$$2K_{vir} + W_{vir} = 0$$

$$E = K_{vir} + W_{vir} = -W_{vir}/2 \approx \frac{GM}{2r_{vir}} = -\frac{GM}{r_{\max}}$$

which implies

$r_{vir} = r_{\max}/2$ ie, 8 times denser than at turnaround

(with a cosmological constant)

$$\ddot{r} = -\frac{GM}{r^2} + \frac{\Lambda}{3}r$$

for EdS, solving this equation gives the density at turnaround as

$$\frac{\rho_{\max}}{\bar{\rho}} \approx 5.5$$

R. Wechsler: lecture notes

The 'tophat model' (spherical collapse)

- consider a uniform, spherical perturbation

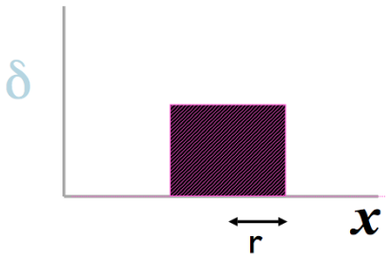

$\delta_i = \rho(t_i)/\rho_b(t_i) - 1$

$M = \rho_b(4\pi r_i^3/3)(1+\delta_i)$

R. Wechsler: lecture notes

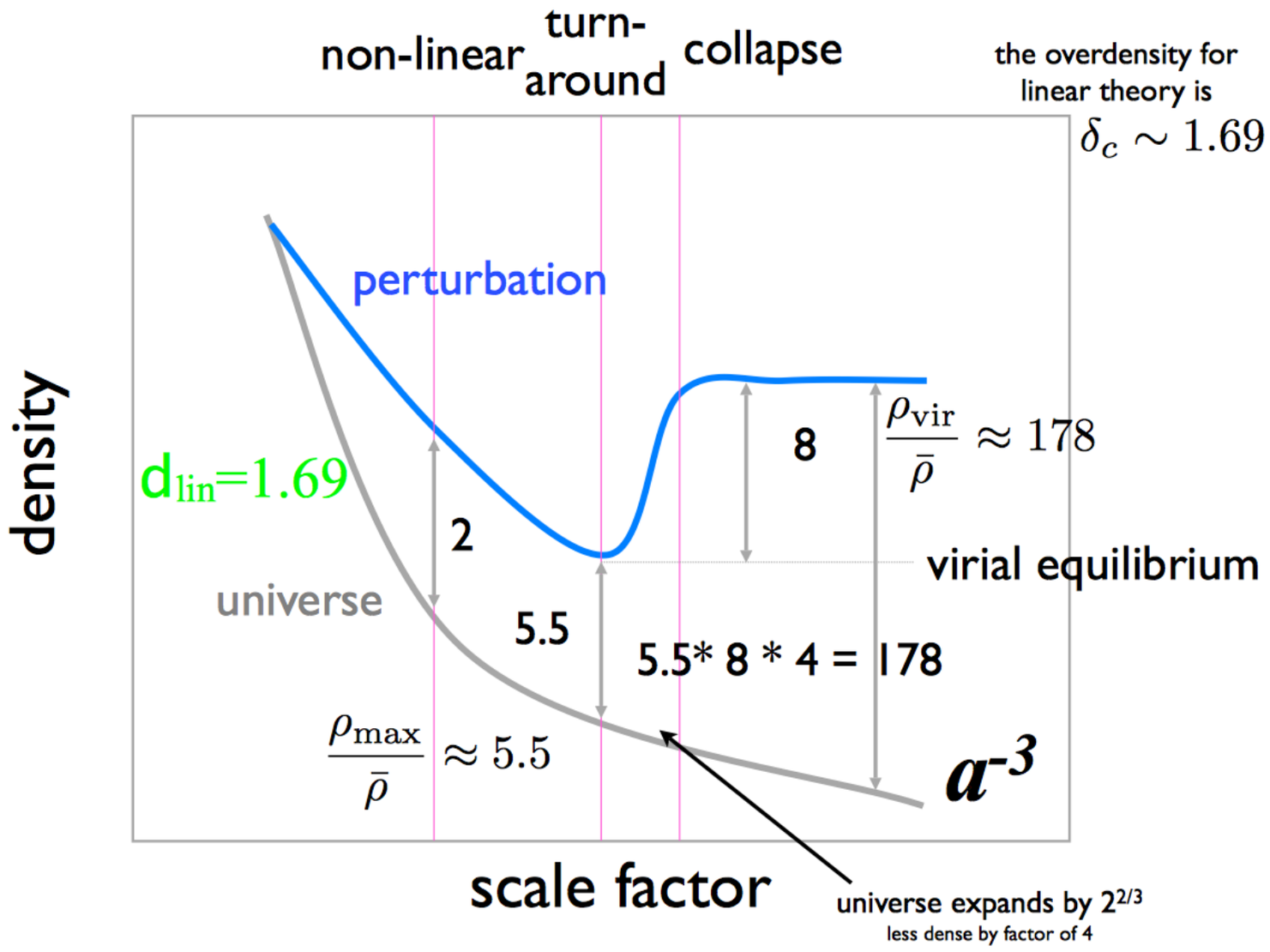

Lesson: time of collapse of a halo depends on the amplitude of fluctuations σ

as estimated by the rms fluctuations of density field smoothed by the top-hat filter with mass M:

$$\sigma^2(M) = \frac{b^2(z)}{2\pi^2}\int_0^\infty k^2 P(k) W^2(k;M)\,\mathrm{d}k.$$

Lesson: time of collapse of a halo depends on the amplitude of fluctuations σ

as estimated by the rms fluctuations of density field smoothed by the top-hat filter with mass M:

$$\sigma^2(M) = \frac{b^2(z)}{2\pi^2} \int_0^\infty k^2 P(k) W^2(k; M)\, \mathrm{d}k.$$

Linear Power spectrum of fluctuations **P(k)** normalized at z=0

Linear growth factor: **b(z=0)** =1

Important: all quantities (such as P(k), b(z)) are estimated by the linear theory, yet the predictions are for the number of halos, which are strongly non-linear objects.

Collapse does not happen as the top-hat model predicts. It is a very non-spherical, extended in time, and complex process. The top-hat model does not describe any of those features.

The top-hat model gives the scaling: halo mass function should depend on σ , not on mass and redshift. Indeed, the mass function dn/dM is very complex if it is expressed as a function of M and z.

However, dn/dM(σ) is also not simple and requires extensive simulations that are used to make accurate approximations. It took ~20 years to produce those approximations.

Abundance of dark matter halos: simple analytical estimates

Dependance of halo cumulative mass function of mass and redshift:

- very steep increase in (n>M) for rare objects
- for sigma ~1 objects the number-density flattens out and declines

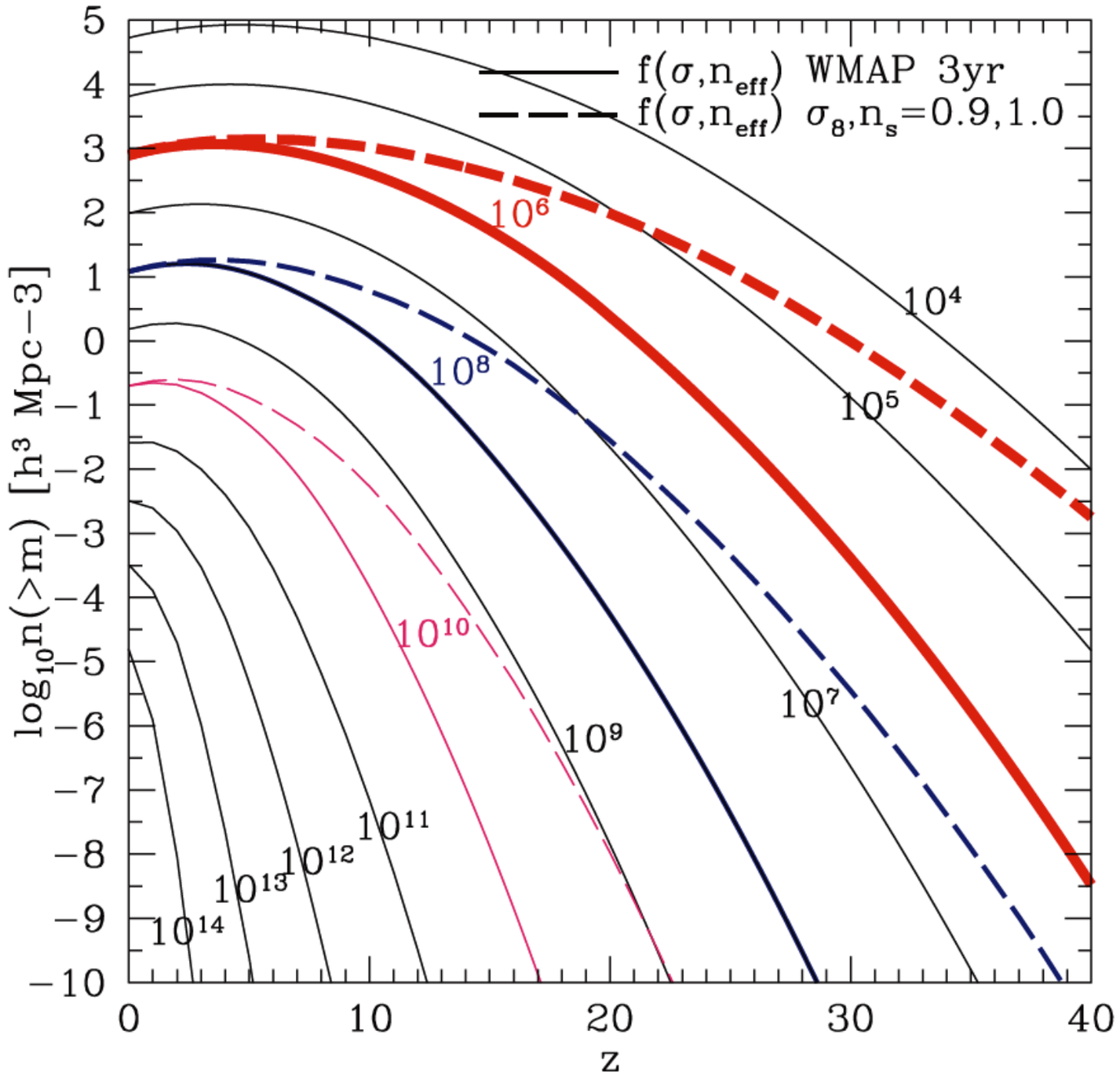

Functional form for mass function:

$$\frac{dn}{dM} = f(\sigma)\,\frac{\bar{\rho}_m}{M}\,\frac{d\ln\sigma^{-1}}{dM}$$

Average matter density:

$$\bar{\rho}_m(z) \equiv \Omega_m(z)\rho_{\rm crit}(z) = \bar{\rho}_m(0)(1+z)^3$$

Numerical factor:

$$f_{\rm P-S}(\sigma) = \sqrt{\frac{2}{\pi}}\,\frac{\delta_{\rm c}}{\sigma}\exp\left(-\frac{\delta_{\rm c}^2}{2\sigma^2}\right)$$

$$\delta_{\rm c} = 1.686$$

$$f_{\rm S-T}(\sigma) = A\sqrt{\frac{2a}{\pi}}\left[1+\left(\frac{\sigma^2}{a\delta_{\rm c}^2}\right)^p\right]\frac{\delta_{\rm c}}{\sigma}\exp\left(-\frac{a\delta_{\rm c}^2}{2\sigma^2}\right)$$

$$A = 0.3222,\ a = 0.707 \text{ and } p = 0.3$$

rms density fluctuation:

$$\sigma^2(M) = \frac{b^2(z)}{2\pi^2}\int_0^\infty k^2 P(k) W^2(k;M)\,{\rm d}k,$$

Galaxy luminosity function

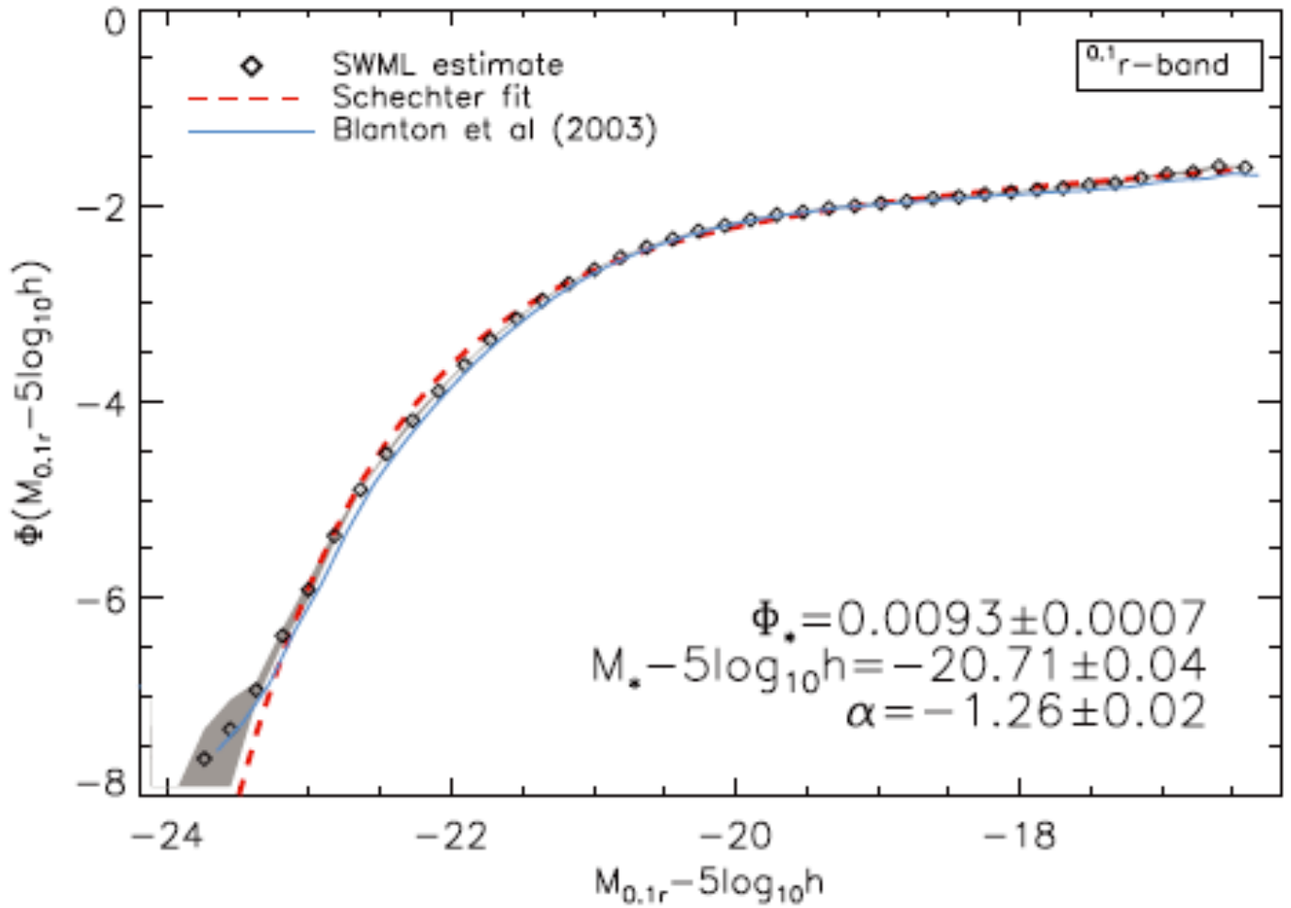

Figure 7. The $^{0.1}r$-band SDSS DR6 LF. The SWML LF estimate is shown in diamonds. The dashed line represents the best-fitting Schechter function and the solid line, the $^{0.1}r$-band LF from Blanton et al. (2003a). Best-fitting values of Schechter parameters α, M_* and Φ_* are also shown in the figure. Shaded regions represent the 1σ uncertainty calculated using a bootstrapping technique.

The Schechter luminosity function

$$\Phi(L) = \left(\frac{\Phi^*}{L^*}\right)\left(\frac{L}{L^*}\right)^{\alpha} \exp\left(-\frac{L}{L^*}\right)$$

number-density of:

Milky-Way type galaxies $n \simeq 10^{-2}\,\mathrm{Mpc}^{-3}$
clusters of galaxies $n \simeq 10^{-6}\,\mathrm{Mpc}^{-3}$
one object $n \simeq 10^{-10}\,\mathrm{Mpc}^{-3}$

A convenient approximation to the luminosity function was suggested by Paul Schechter in 1976.

In this expression:

- ϕ^* is a normalization factor which defines the overall density of galaxies (number per cubic Mpc)
- L* is a characteristic galaxy luminosity. An L* galaxy is a bright galaxy, roughly comparable in luminosity to the Milky Way. A galaxy with $L < 0.1\ L^*$ is a dwarf.
- α defines the `faint-end slope' of the luminosity function. a is typically negative, implying large numbers of galaxies with low luminosities.

Galaxy stellar mass function

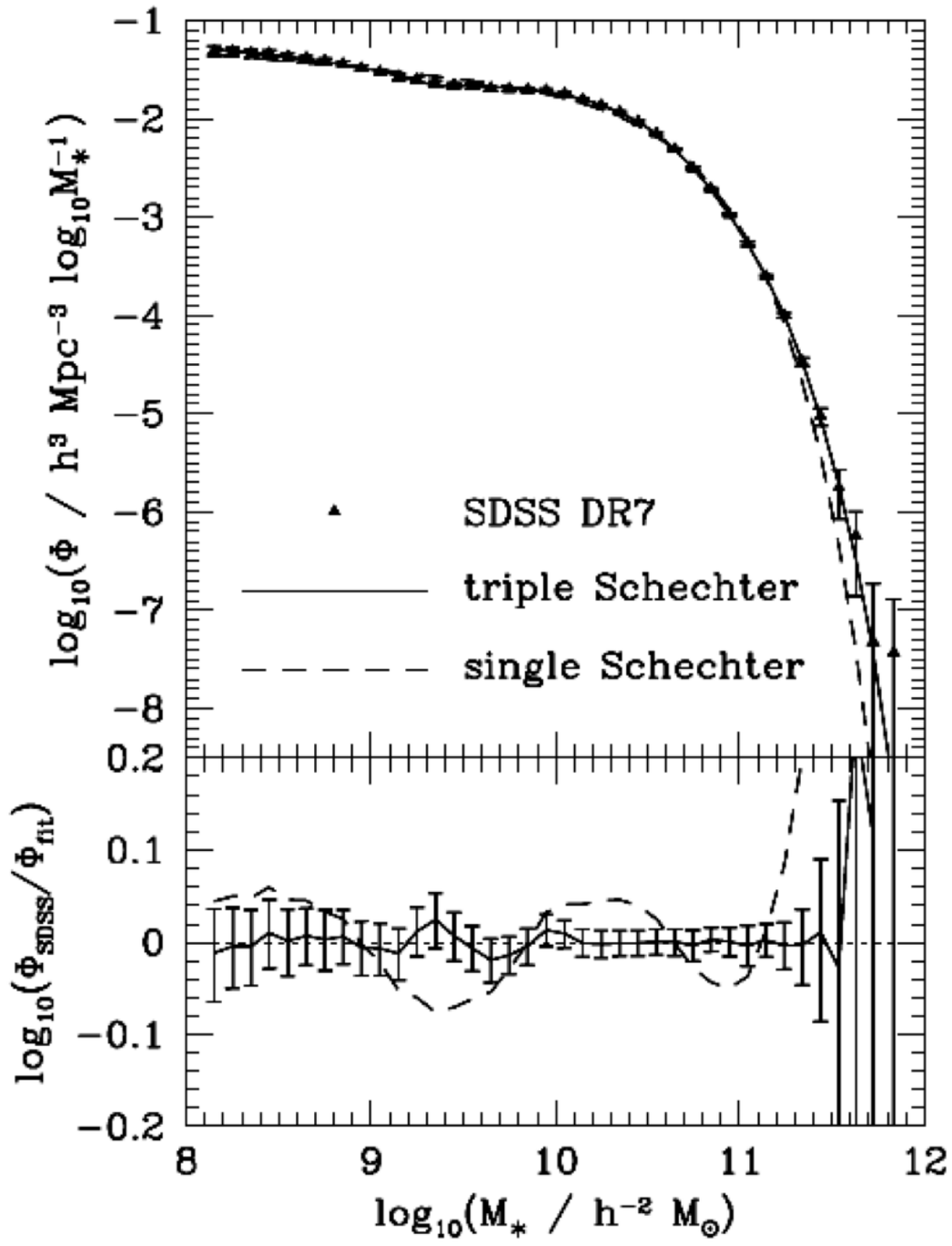

Halo mass function

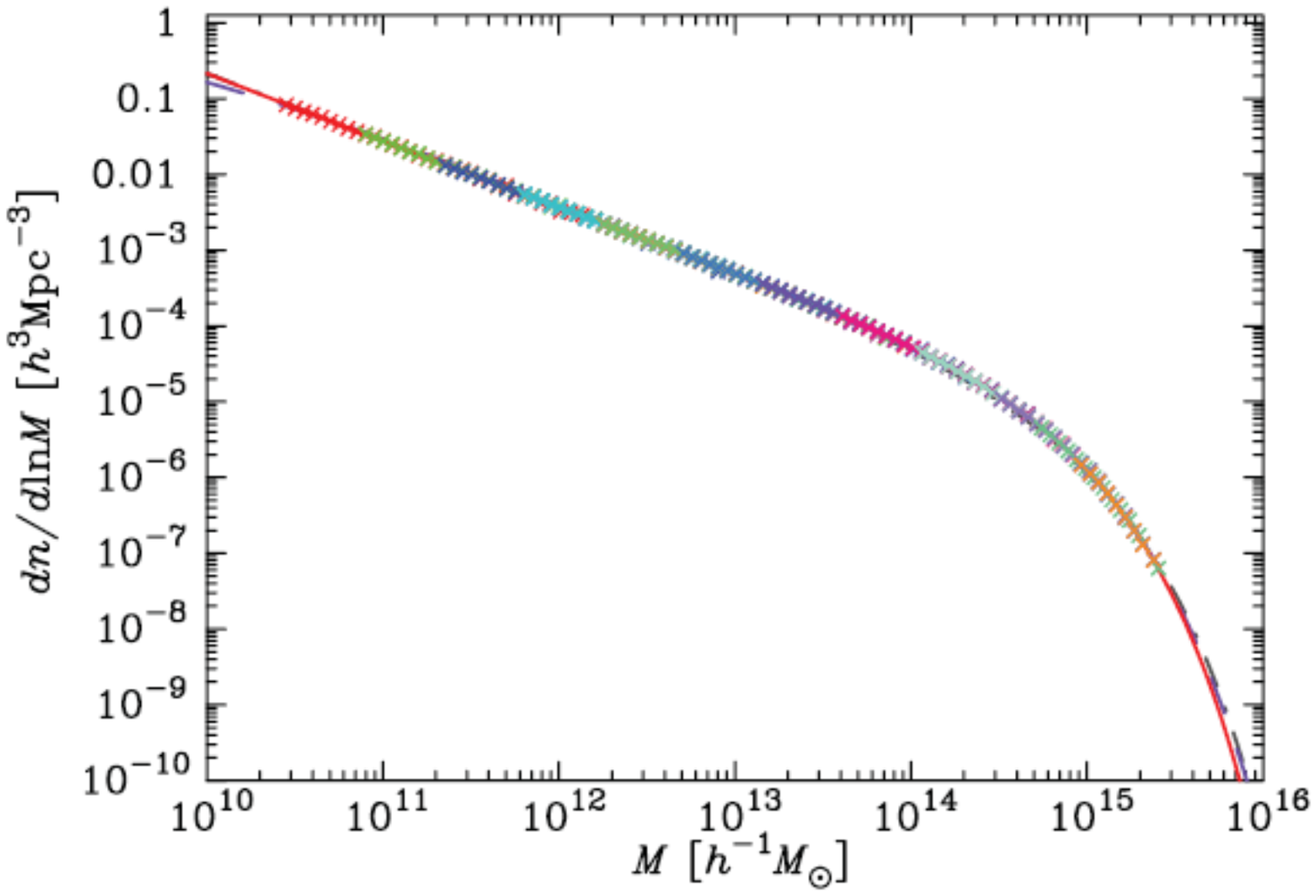

FIG. 1.—Central values of the binned mass functions from sixteen 1024^3 simulations of the ΛCDM universe as crosses, with simulations in different colors. The best-fit form for the mass function we calculate is shown as a solid line (*red*), the Jenkins fit as a dashed line (*purple*), and the Sheth-Tormen fit as a dot-dashed line (*dark gray*). Goodness of fit is poorly judged on this extreme log scale; it is more clearly resolved in the linear residuals of Fig. 2.

Warren et al 2006

Halo mass function at z=0

Note the vertical axis scaling: the main trend of the mass function - $dn/dM \sim M^{-2}$ - has been taken away. We are looking at the deviations from the power-law.

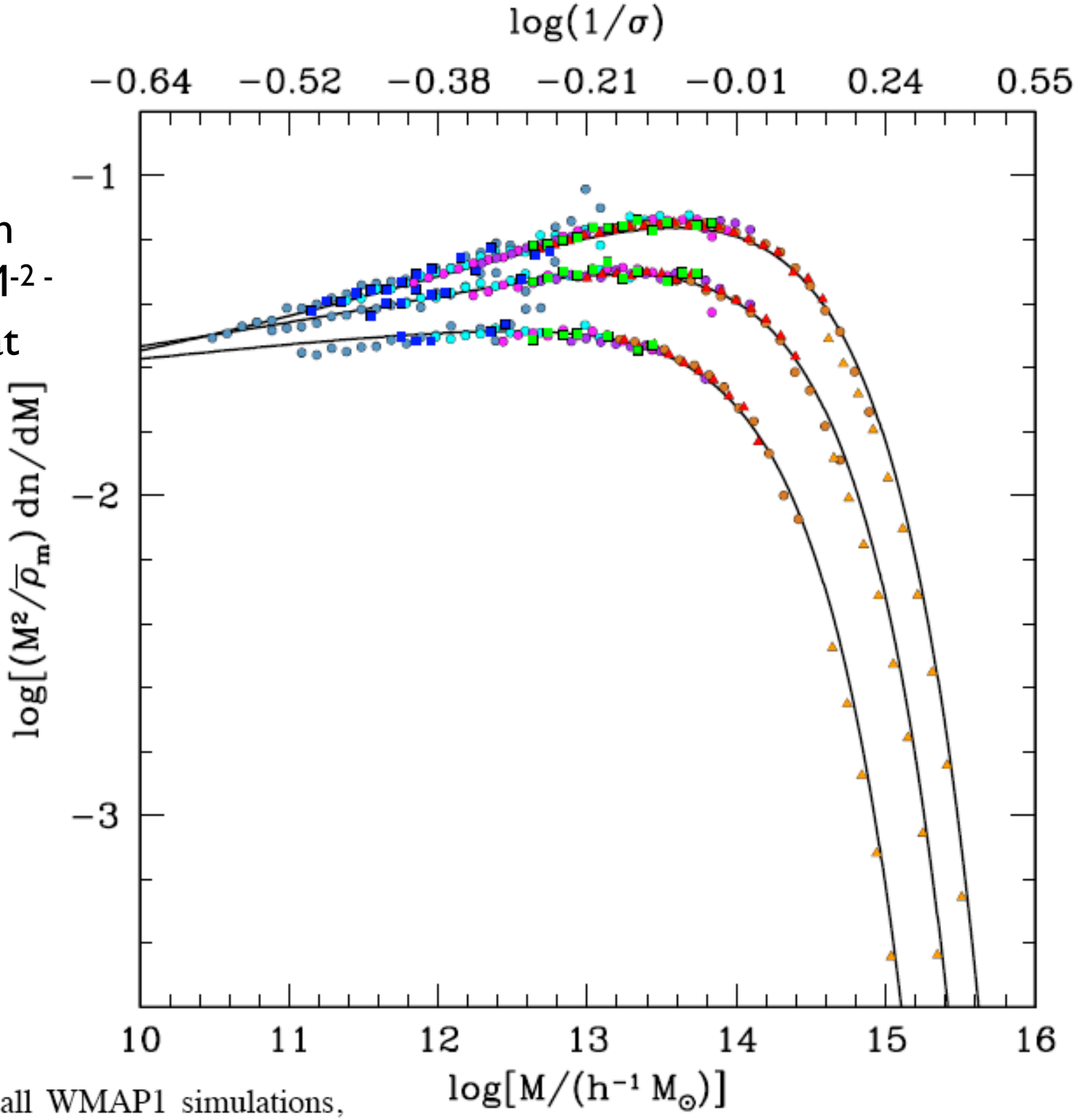

FIG. 5.— The measured mass functions for all WMAP1 simulations, plotted as $(M^2/\bar{\rho}_m)dn/dM$ against $\log M$. The solid curves are the best-fit functions from Table 2. The three sets of points show results for $\Delta = 200$, 800, and 3200 (from top to bottom). To provide a rough scaling between M and σ^{-1}, the top axis of the plot shows σ^{-1} for this mass range for the WMAP1 cosmology. The slight offset between the L1280 results and the solid curves is due to the slightly lower value of $\Omega_m = 0.27$.

Tinker etal 2008

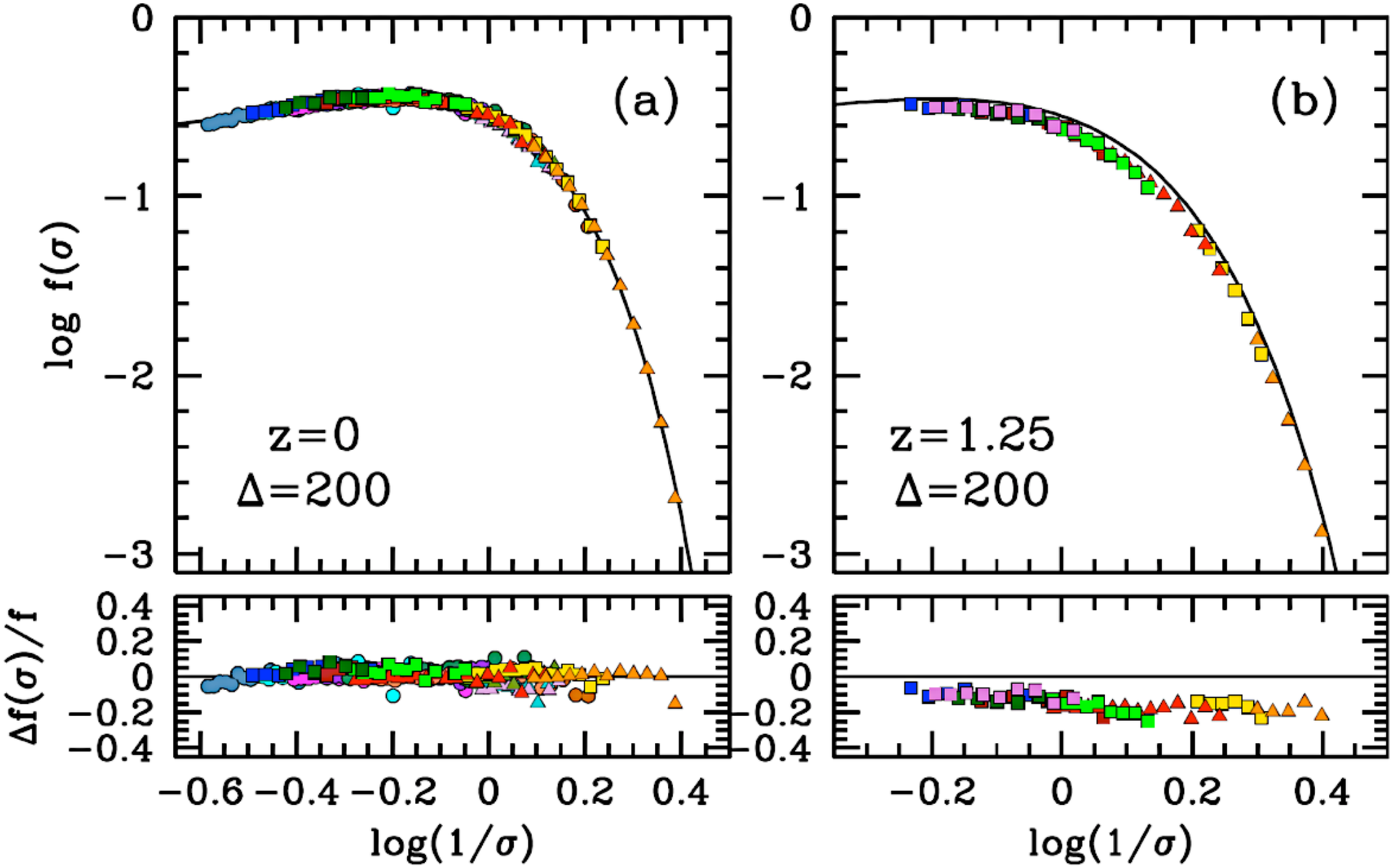

Nearly universal shape of mass function when we plot $f(\sigma)$

$$\frac{dn}{dM} = f(\sigma)\,\frac{\bar{\rho}_m}{M}\,\frac{d\ln\sigma^{-1}}{dM}$$

Evolution of the mass function with redshift

Full curves are for the Sheth-Torman approximation

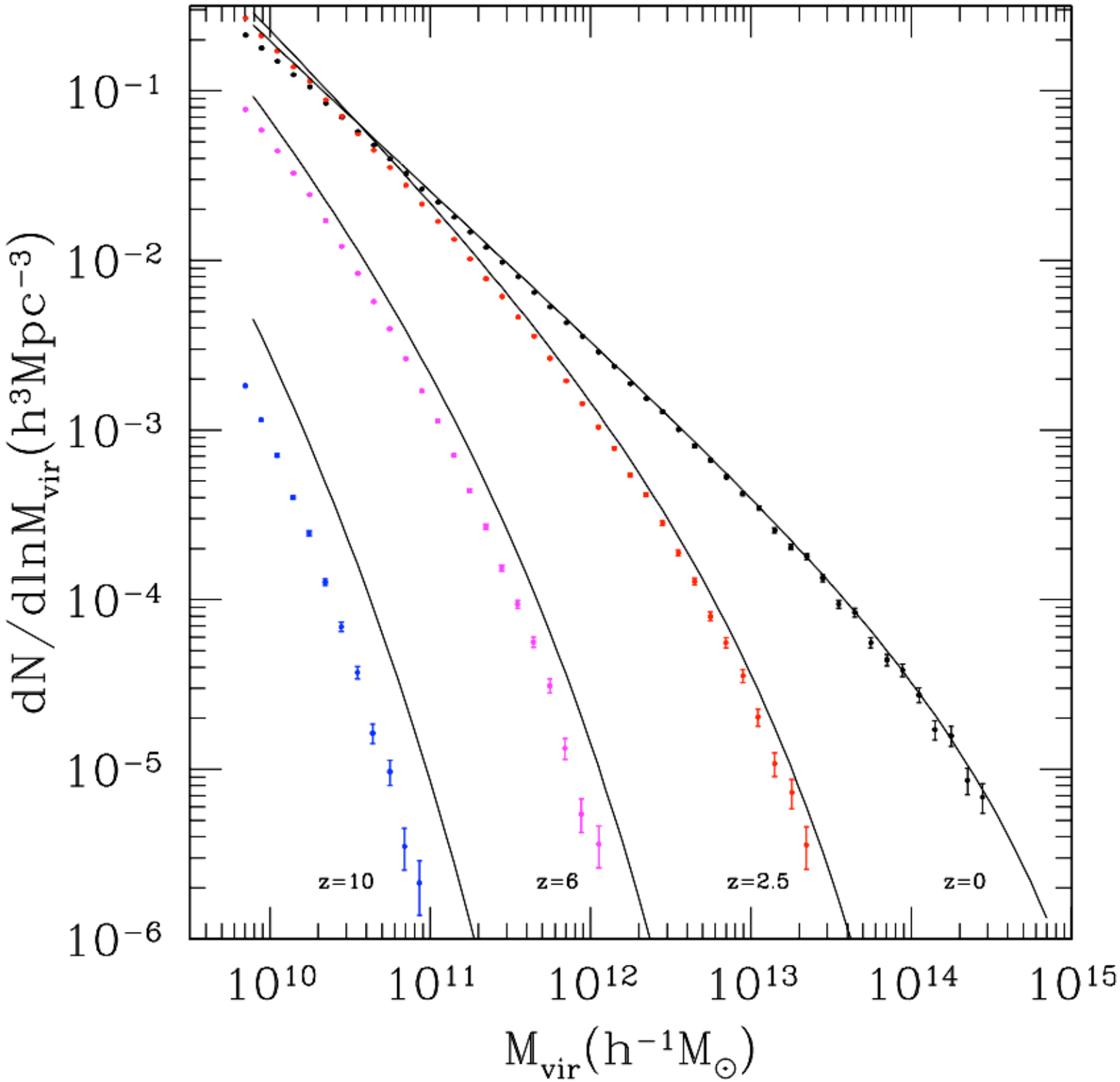

Symbols are from N-body simulations for distinct halos defined using Spherical Overdensity algorithm

Halo Velocity function

For each halo we find mass within given radius
M(<r) and then find maximum of circular velocity

$$V_{\rm circ} = \sqrt{\frac{GM(<r)}{r}}\Big|_{\rm max}$$

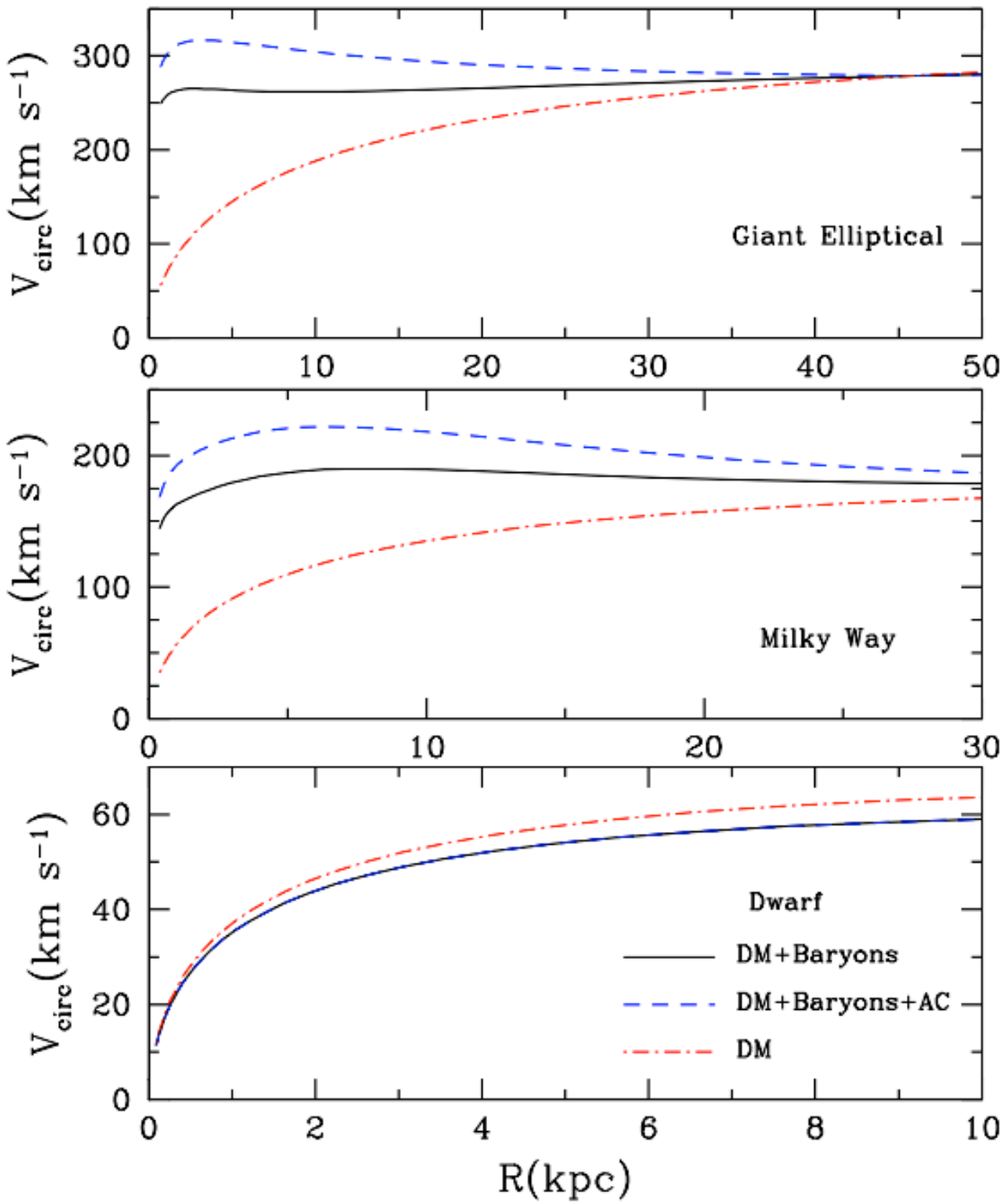

Fig. 5.— Effect of cold baryons on circular velocity profiles for three characteristic models of galaxies with virial masses 10^{13} $M_\odot$ (top), 1.7×10^{12} $M_\odot$ (middle), and 7×10^{10} $M_\odot$ (bottom). The "DM" curves include a cosmological fraction of baryons that trace the dark matter distribution. The cold baryon mass is added to the true dark matter mass in calculating the circular velocity ("DM+Baryons"). The effect of adiabatic compression of the dark matter is included in the models named "DM+Baryons+AC". After adding the cold baryons the circular velocities are rather flat in the inner $5 - 10$ kpc regions.

Halo Velocity function

$$n(>V) = AV^{-3}\exp\left(-\left[\frac{V}{V_0}\right]^{\alpha}\right)$$

$V_0 = 800$ km s^{-1}.

where the parameters A, V_0, and α are functions of redshift. For $z = 0$ we find

$$A = 1.82 \times 10^4 (h^{-1}\ \mathrm{Mpc/km\ s^{-1}})^{-3},$$
$$\alpha = 2.5, \qquad (16)$$

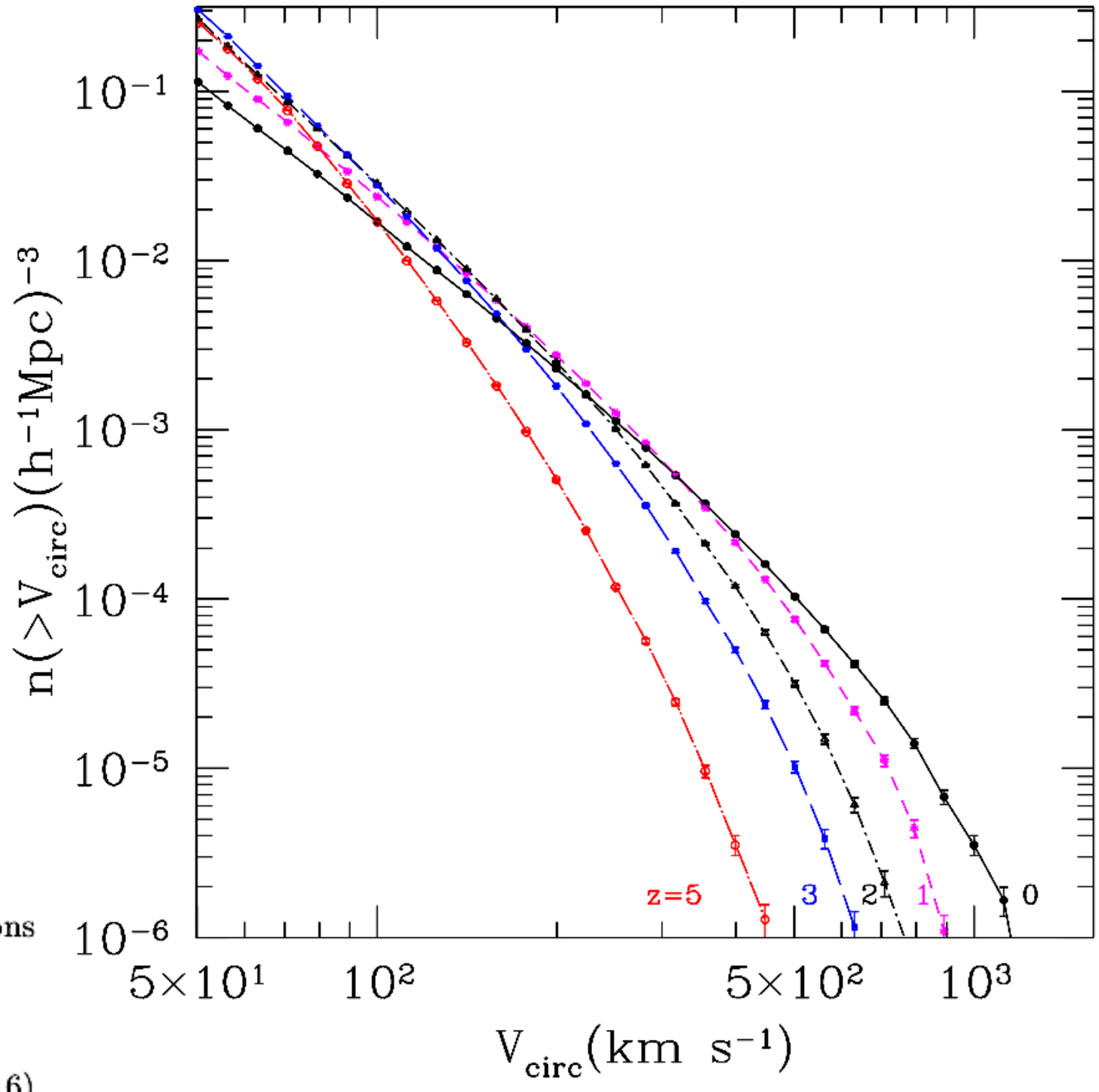

Warm dark matter

Simulation	$m_{\rm WDM}$ [keV]
CDM-W7	–
$m_{2.3}$	2.322
$m_{2.0}$	2.001
$m_{1.6}$	1.637
$m_{1.5}$	1.456

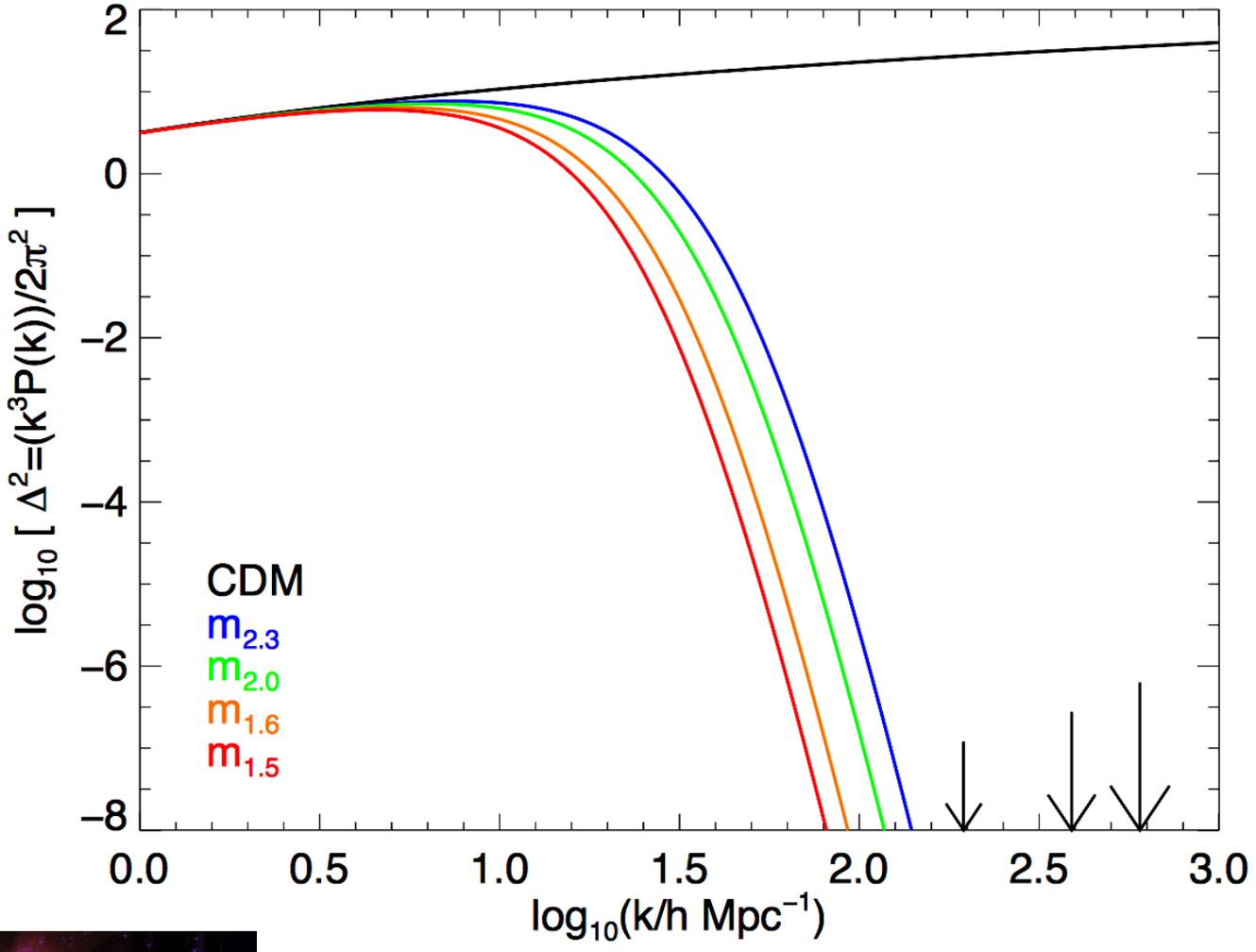

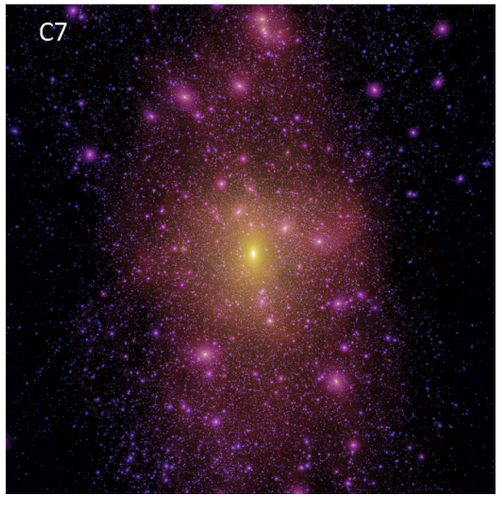

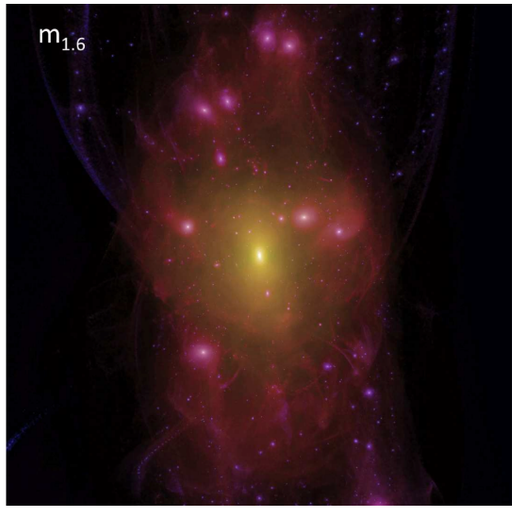

Lovell et al 2014

Wang & White 2007.
Even with 512 particles the filament is highly fragmented.

The 256 and 128 configurations were plain horrible

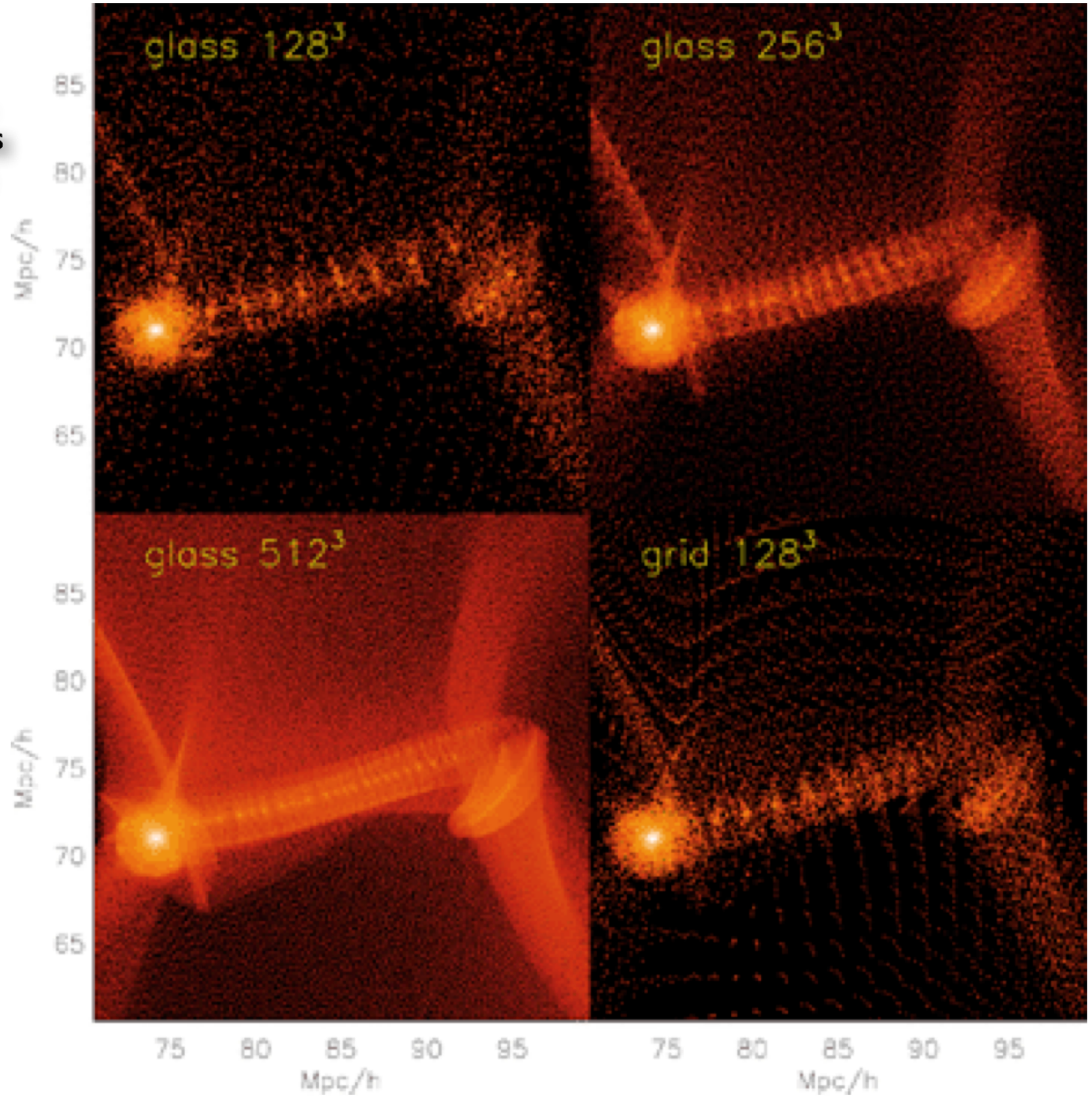

WDM VF (Schneider et al 2013)

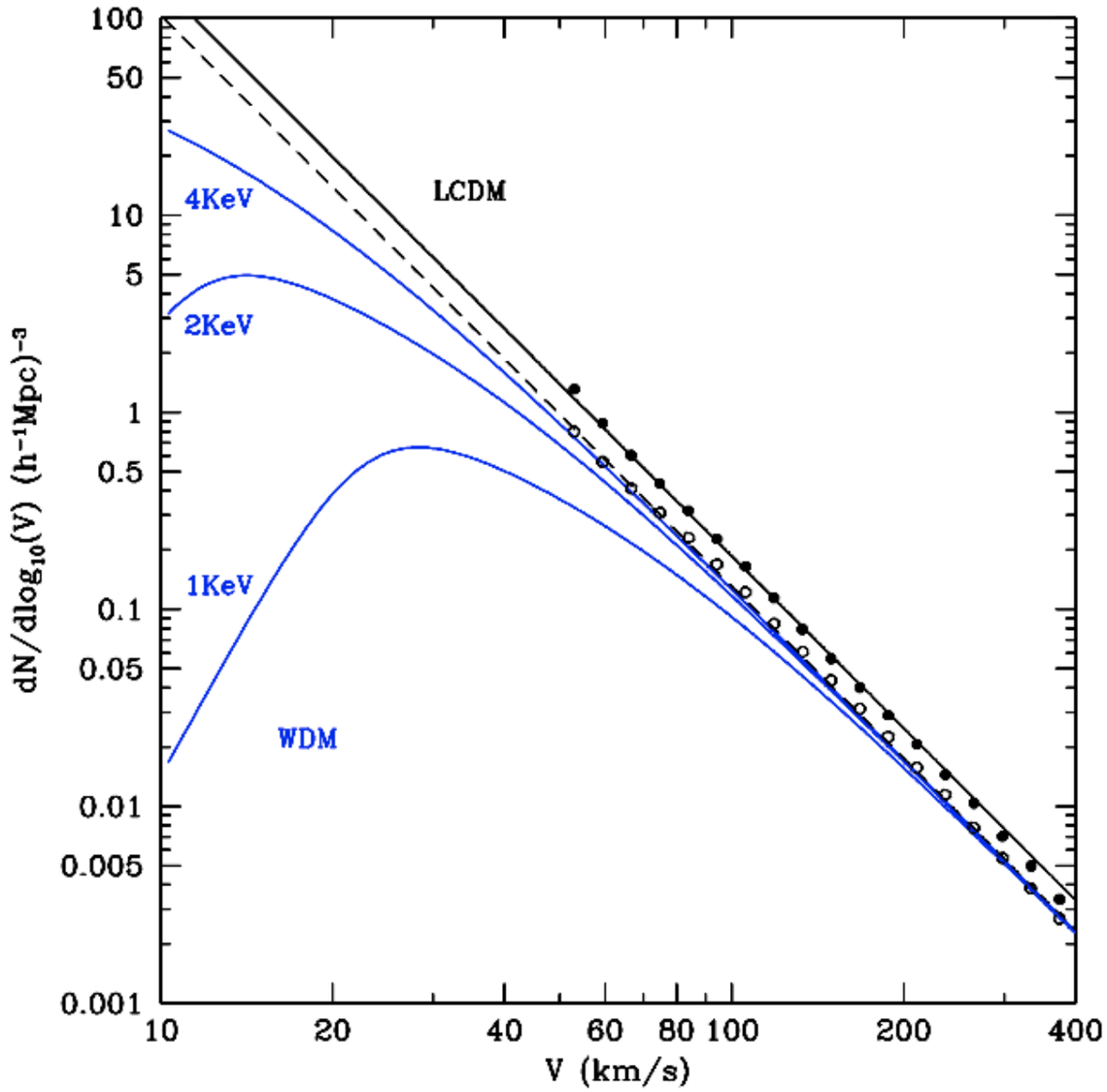

Klypin, Karachentsev, Makarov 2014

Abundance of Field Galaxies

Goals:

Observational measurements of Galaxy Velocity Function for a sample, which is not HI-selected and includes all types of galaxies

Local Volume:

600 dwarf galaxies

- most are not satellites
- early and late types
- HI line widths and vel. dispersions.
- D< 10 Mpc

Klypin, Karachentsev, Makarov 2014

Abundance of Field Galaxies

Local Volume: **Not corrected for inclination**

600 dwarf galaxies
- most are not satellites
- early and late types
- HI line widths and vel. dispersions.
- D< 10 Mpc

Consistent results:
Local Volume is 10% above HI surveys because it has early type galaxies

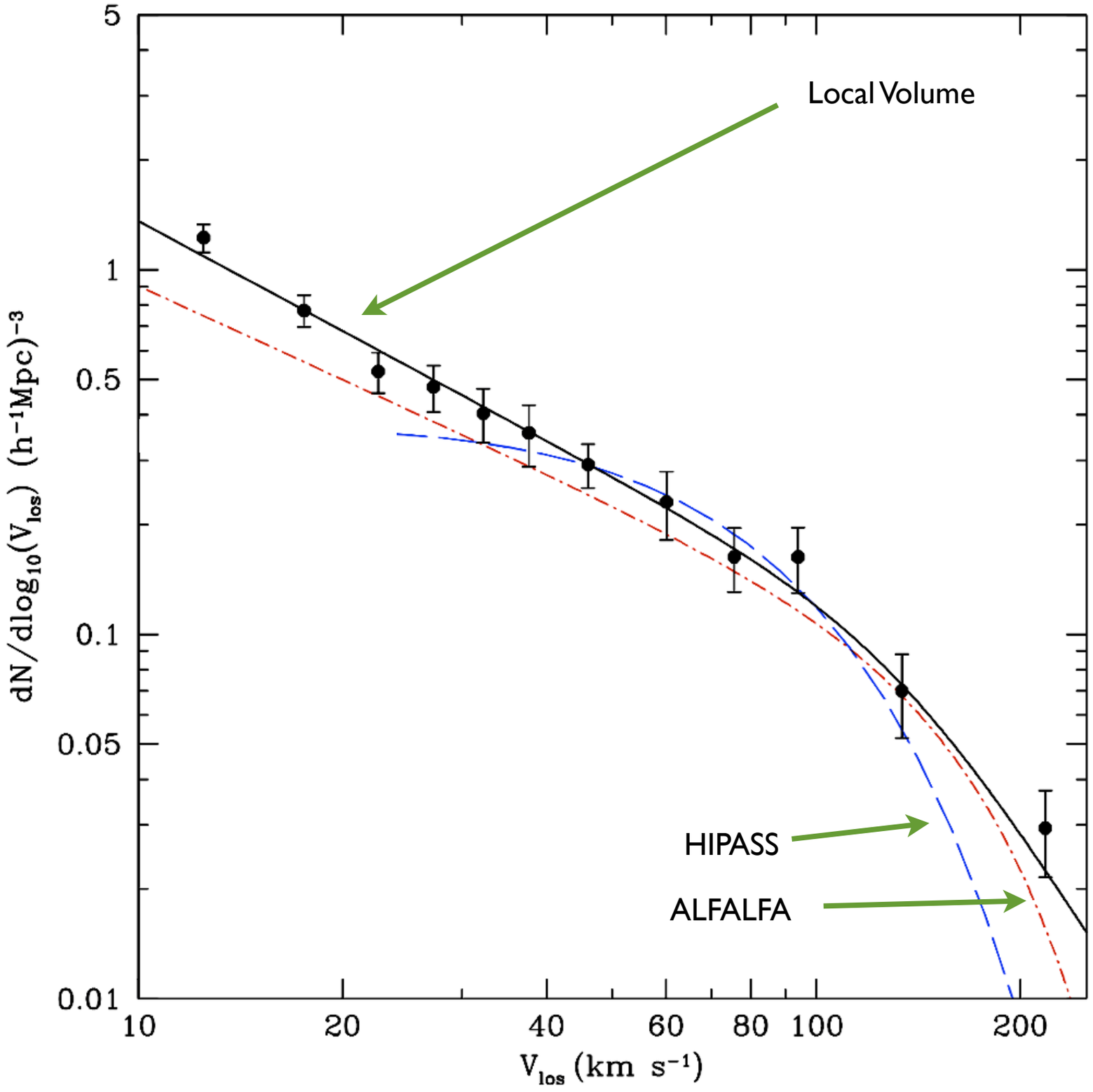

Klypin, Karachentsev, Makarov 2014

Abundance of Field Galaxies

Local Volume:

600 dwarf galaxies
- most are not satellites
- early and late types
- HI line widths and vel. dispersions.
- D< 10 Mpc

LCDM: - Planck cosmology
- halos + subhalos
- corrected for baryons
- random disk orientation

Good fit to galaxies with V>60km/s

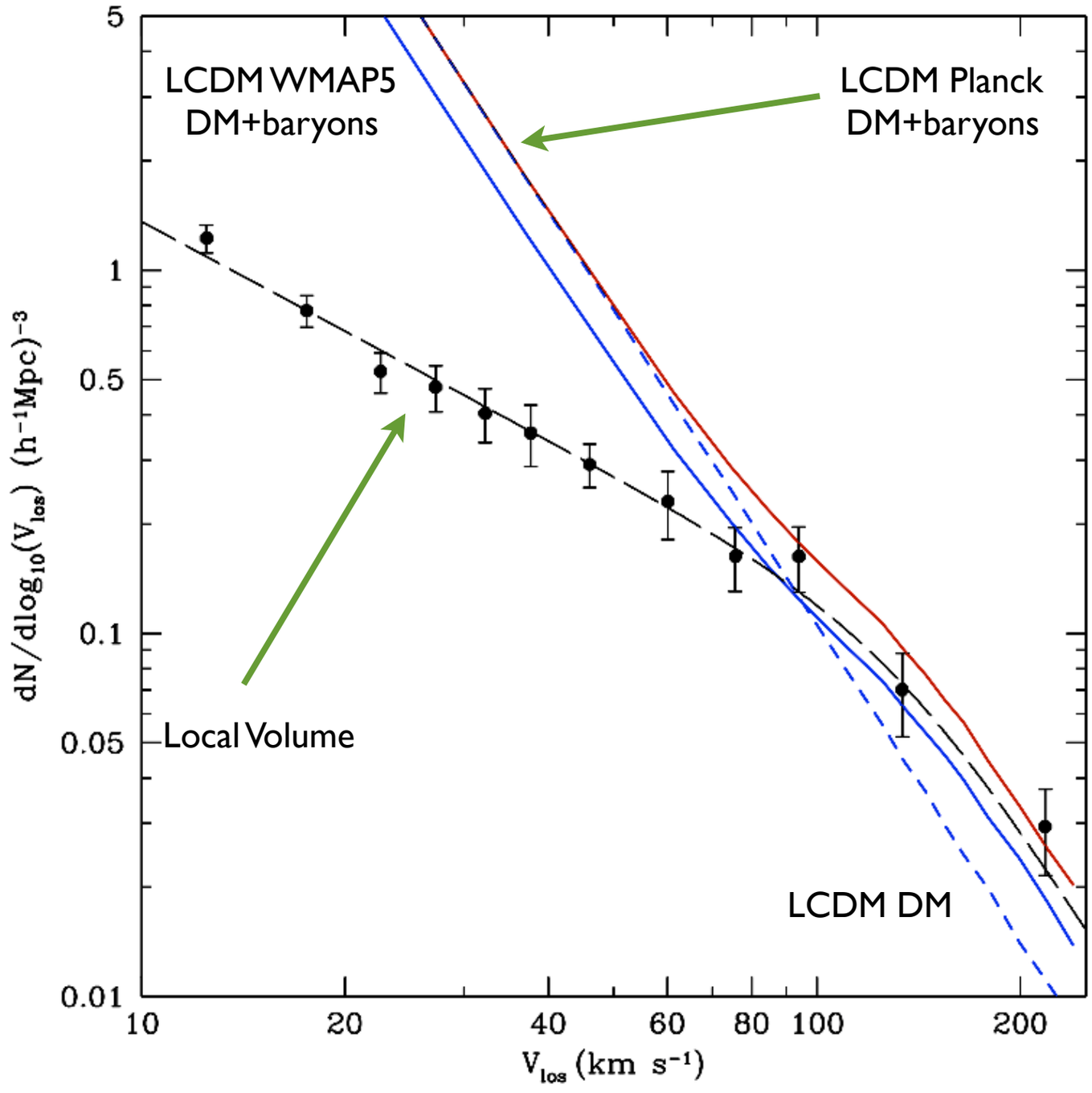

Disagreement 3-5 times for V =30-40km/s

Klypin, Karachentsev, Makarov 2014

Abundance of Field Galaxies

Local Volume:

600 dwarf galaxies
- most are not satellites
- early and late types
- HI line widths and vel. dispersions.
- D< 10 Mpc

WDM: - Scheneider, Dutton&Maccio

used mass function and concentrations for WDM
- Planck cosmology
- halos + subhalos
- corrected for baryons
- random disk orientation

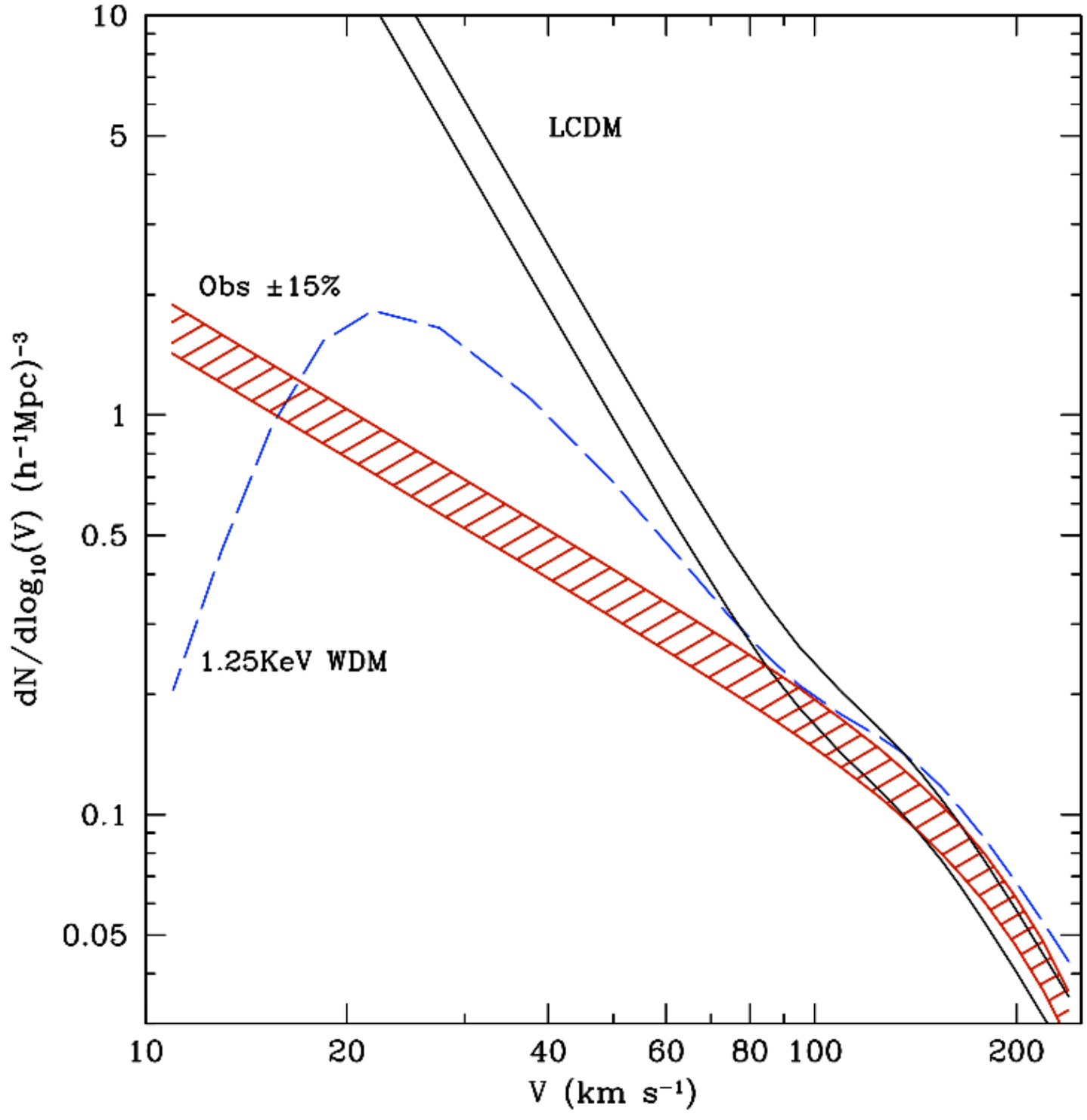

No neutrino mass solves the problem

Brook & Di Cintio 2015

Abundance of Field Galaxies

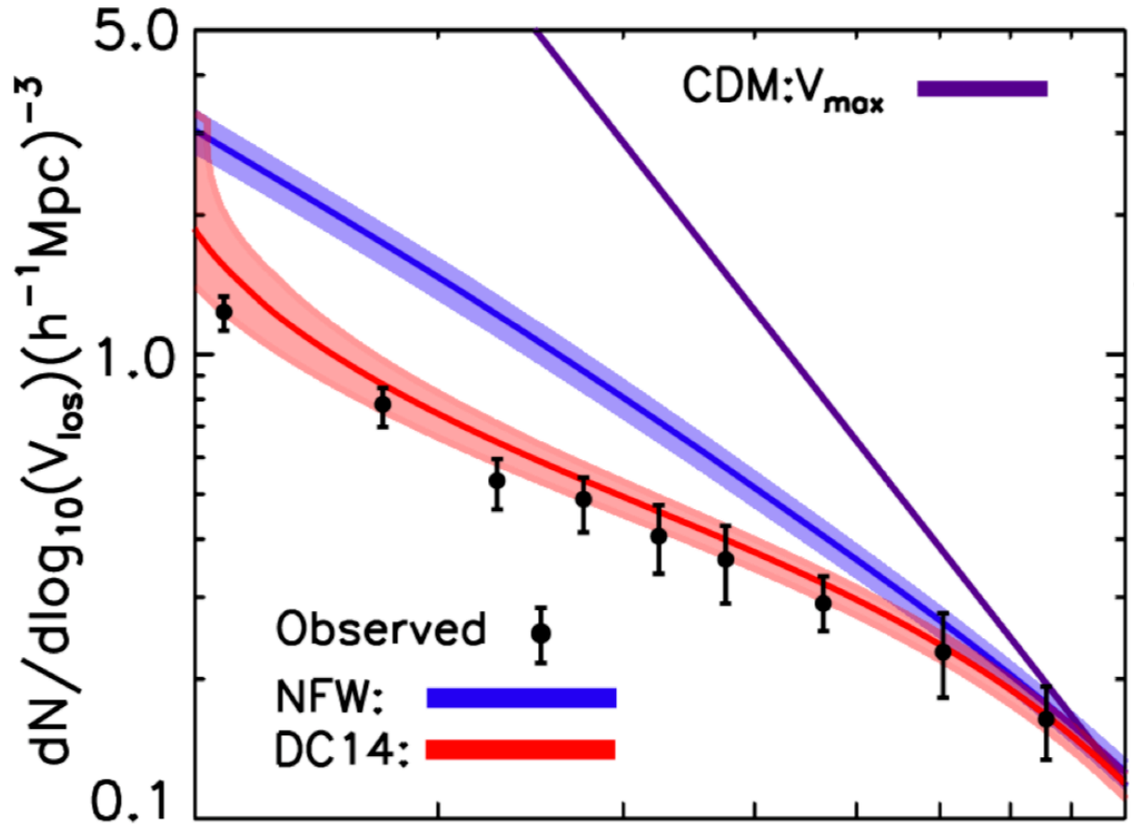

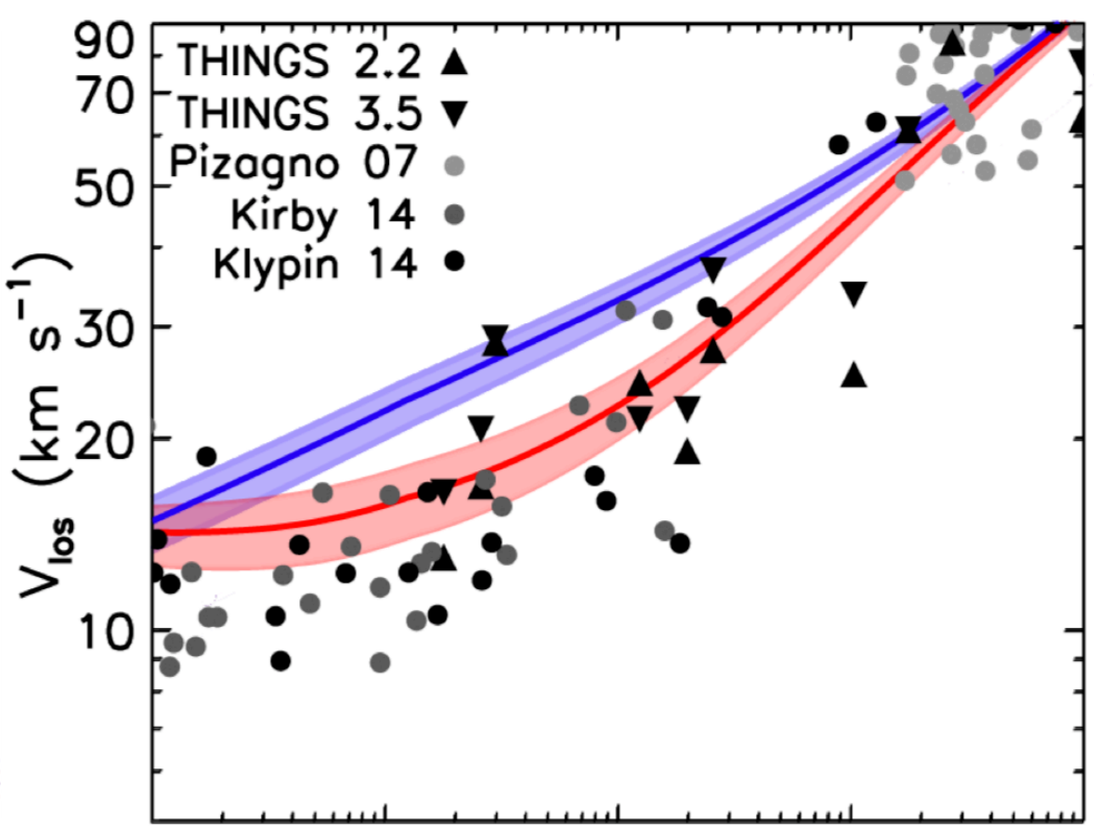

The mass dependent DC14 density profile is based on such cosmological simulations, and accounts for the expansion of dark matter haloes due to the effects of feedback from star forming regions (Di Cintio et al. 2014b). These profiles self consistently account for the distance to which dark matter is moved, addressing the concerns of Maxwell et al. (2015), and take the form:

$$\rho(r) = \frac{\rho_s}{\left(\frac{r}{r_s}\right)^{\gamma}\left[1+\left(\frac{r}{r_s}\right)^{\alpha}\right]^{(\beta-\gamma)/\alpha}} \tag{7}$$

The DC14 model describes profiles that have a range of inner slopes, with the parameters of the double power law model being dependent on the stellar-to-halo mass ratio of a galaxy in the following way (Di Cintio et al. 2014b):

$$\begin{aligned}\alpha &= 2.94 - \log_{10}[(10^{X+2.33})^{-1.08} + (10^{X+2.33})^{2.29}] \\ \beta &= 4.23 + 1.34X + 0.26X^2 \\ \gamma &= -0.06 + \log_{10}[(10^{X+2.56})^{-0.68} + (10^{X+2.56})]\end{aligned} \tag{8}$$

where $X = \log_{10}(\mathrm{M_{star}/M_{halo}})$. The scale radius, r_s, is connected to the concentration of the halo, which varies with mass.

Halos: snapshots

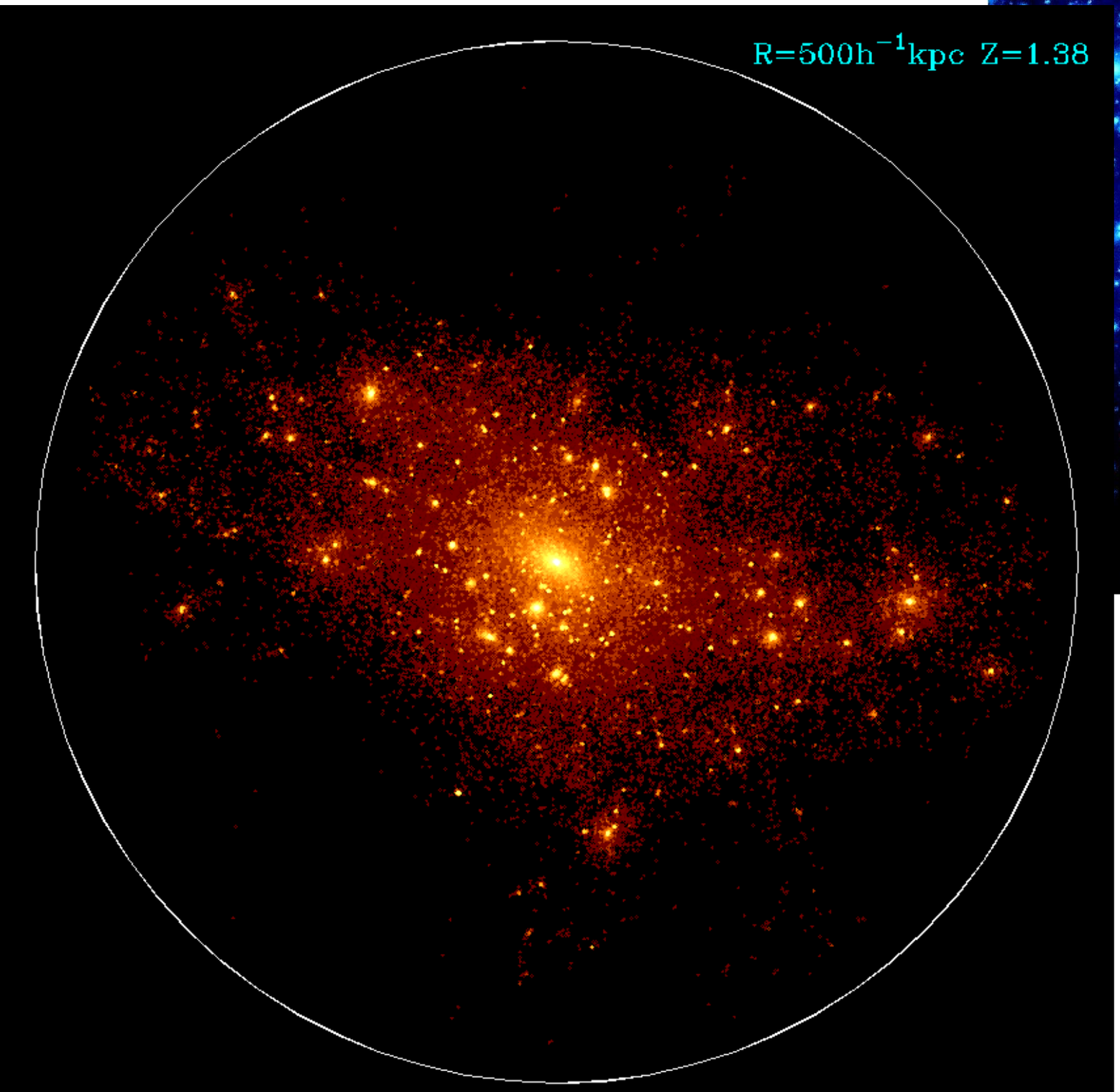

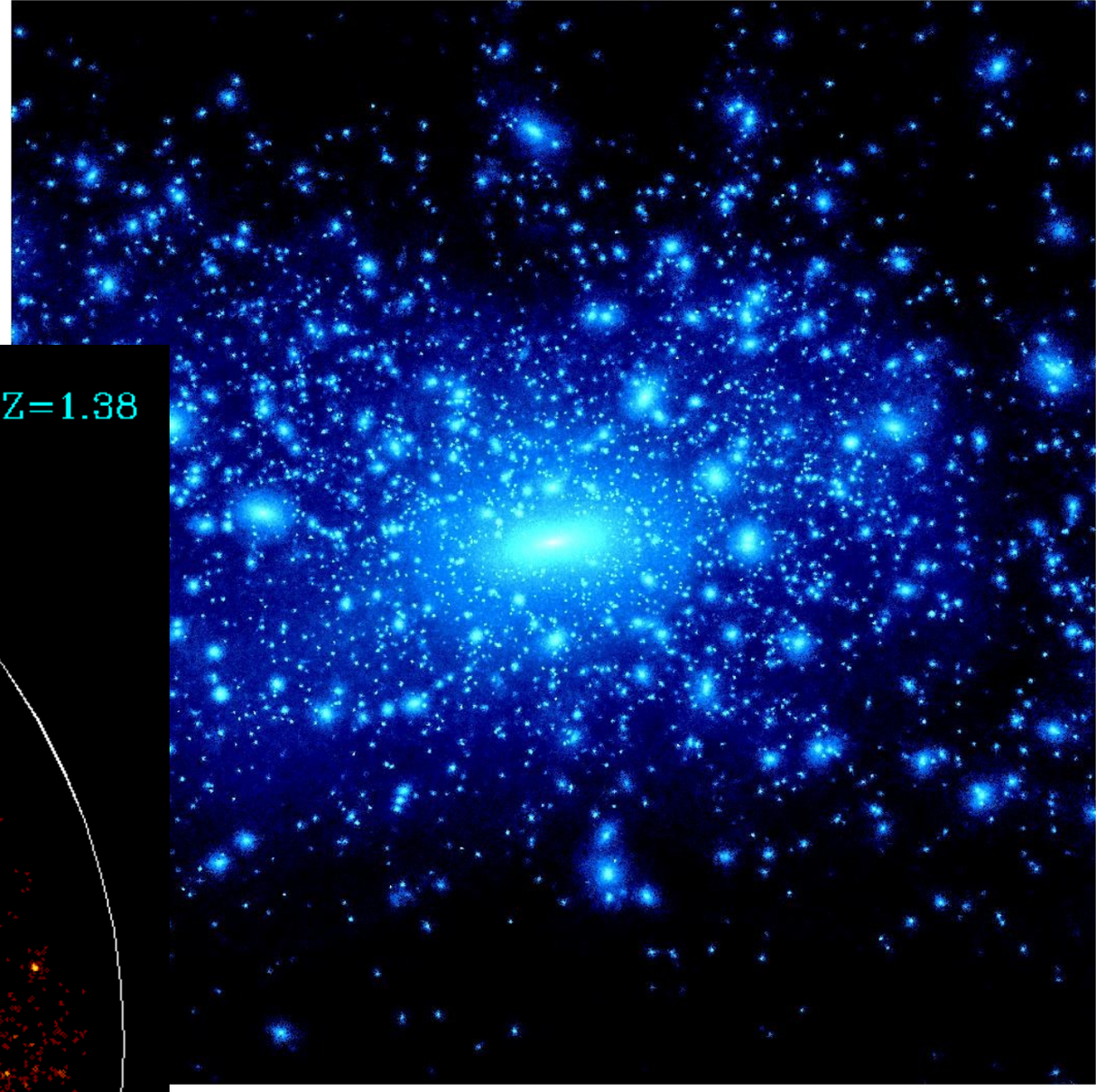

Subhalos

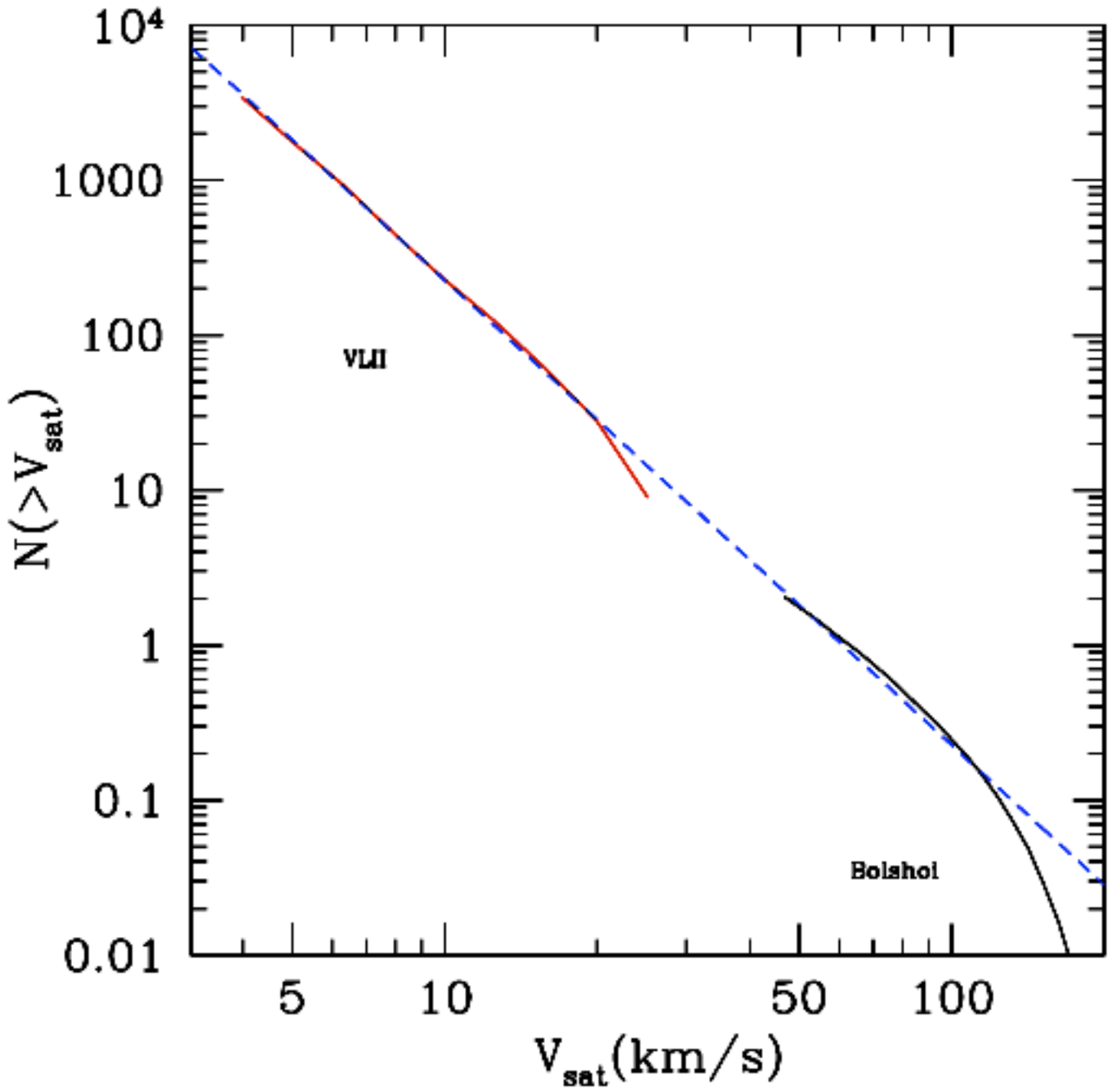

$$N(>x) = 1.7 \times 10^{-3} V_{\rm host}^{1/2} x^{-3},$$

$$x \equiv V_{\rm sub}/V_{\rm host}, \quad x < 0.7,$$

Figure 14. Comparison of satellite velocity functions in the Via Lactea-II and Bolshoi simulations for host halos with $V_{\rm circ} = 200$ km s^{-1} and $M_{\rm vir} \approx 1.3 \times 10^{12}\, h^{-1}\, M_\odot$. The dashed line is a power law with slope -3, which provides an excellent fit to both simulations. In both simulations satellites are found inside a sphere with virial radius $R_{\rm vir}$.

Subhalos

The cumulative velocity function of satellites for host halos with different maximum circular velocities ranging from ≈ 150 km/s to ≈ 1000 km/s– from bottom to top. The panel uses the velocities of subhalos at redshift z = 0.

Larger halos have more sub halos in relative units.

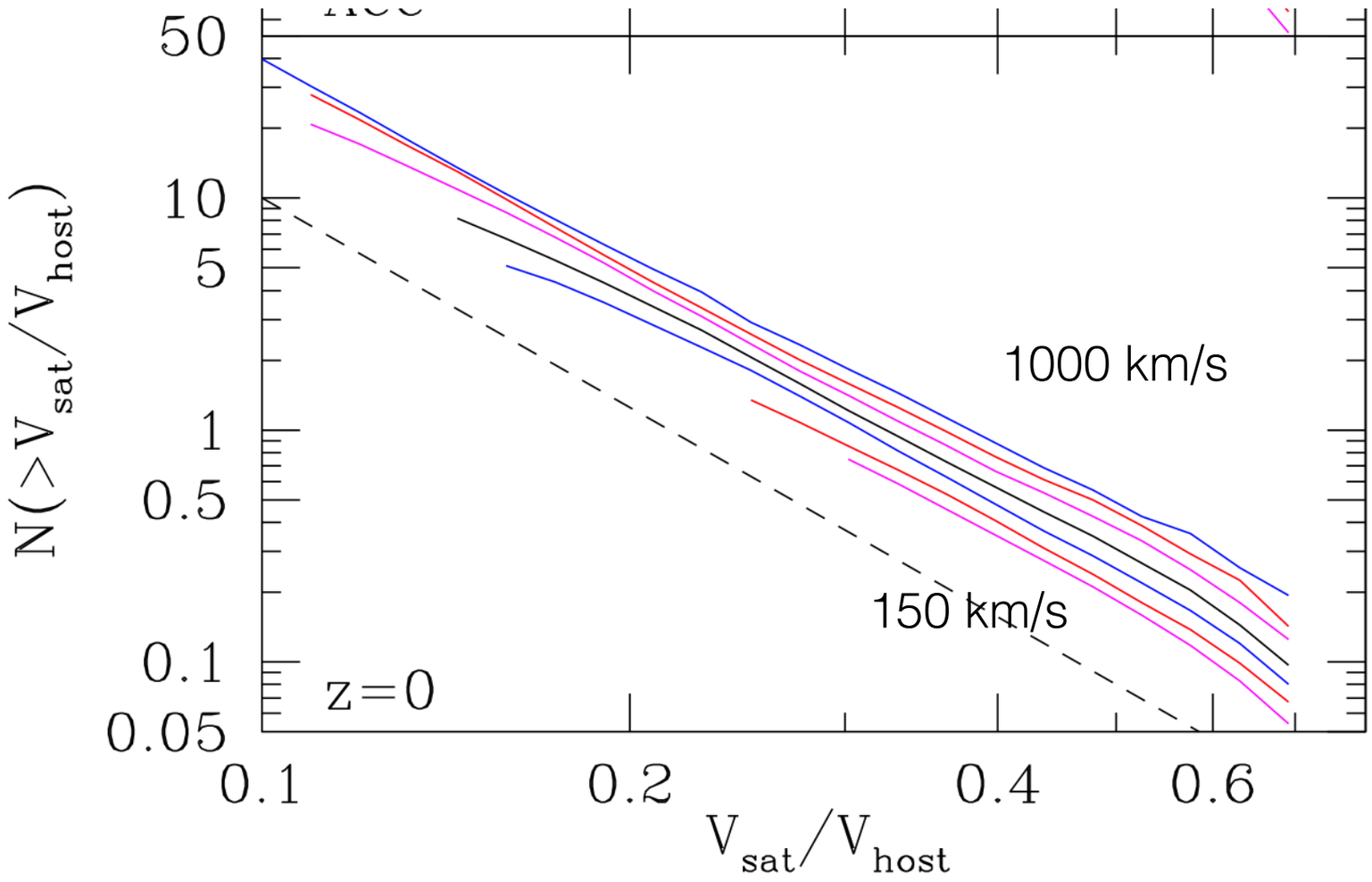

Subhalos

The velocity function of satellites compared with the velocity function of distinct halos. The bottom panel shows the cumulative function of subhalos (bottom full curve) and distinct halos (top full curve). The circular velocity used for the plot is the peak over each halo's history. The dashed curves are analytical approximations. The top panel shows the ratio of the number of subhalos and distinct halos (full curve) and an analytical approximation for the ratio (dashed curve).

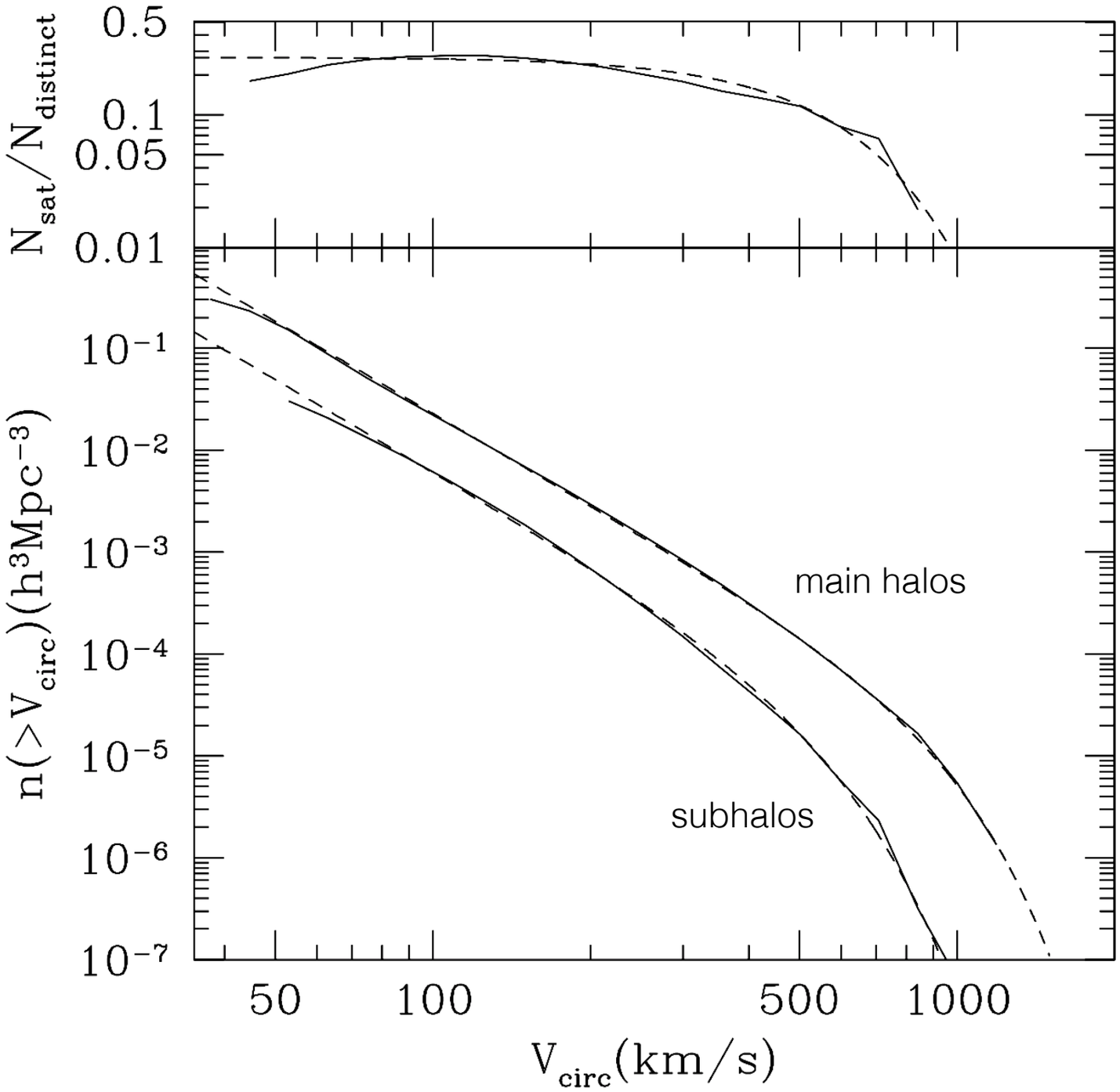

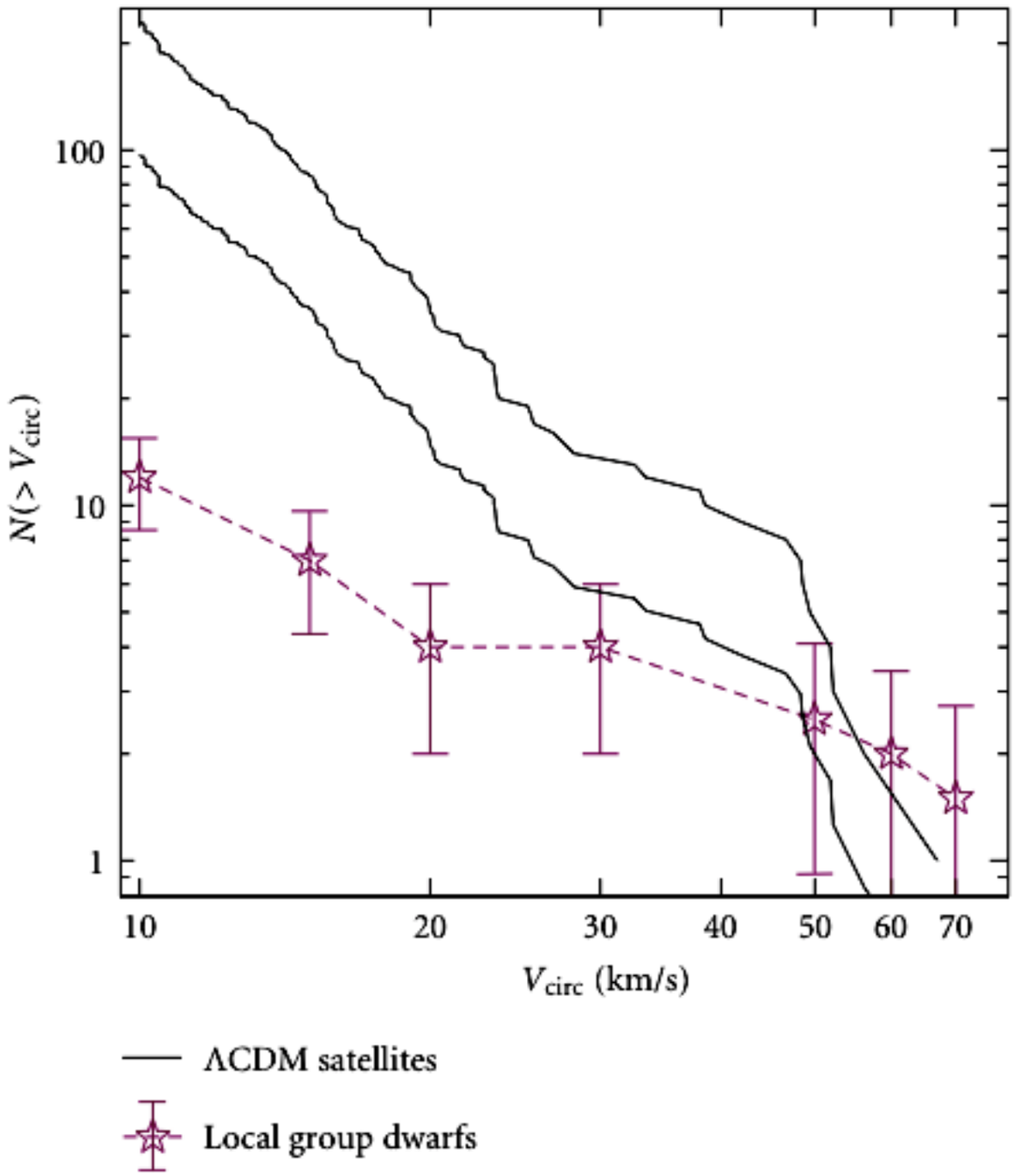

FIGURE 7: Comparison of the cumulative circular velocity functions, $N(> V_{max})$, of subhalos and dwarf satellites of the Milky Way within the radius of 286 kpc (this radius is chosen to match the maximum distance to observed satellites in the sample and is smaller than the virial radius of the simulated halo, $R_{337} = 326$ kpc). The subhalo VFs are plotted for the host halos with maximum circular velocities of 160 km/s and 208 km/s that should bracket the V_{max} of the actual Milky Way halo. The VF for the observed satellites was constructed using circular velocities estimated from the line-of-sight velocity dispersions as $V_{max} = \sqrt{3}\sigma_r$ (see the discussion in the text for the uncertainties of this conversion).

Kravtsov 2009

Kravtsov, Gnedin, Klypin 2004

Klypin et al 1999

Moore et al 1999

Early explanation for the discrepancy was photoionization. Now it is mostly tidal stripping: luminous satellites were much larger in the past. The small one were photo evaporated.

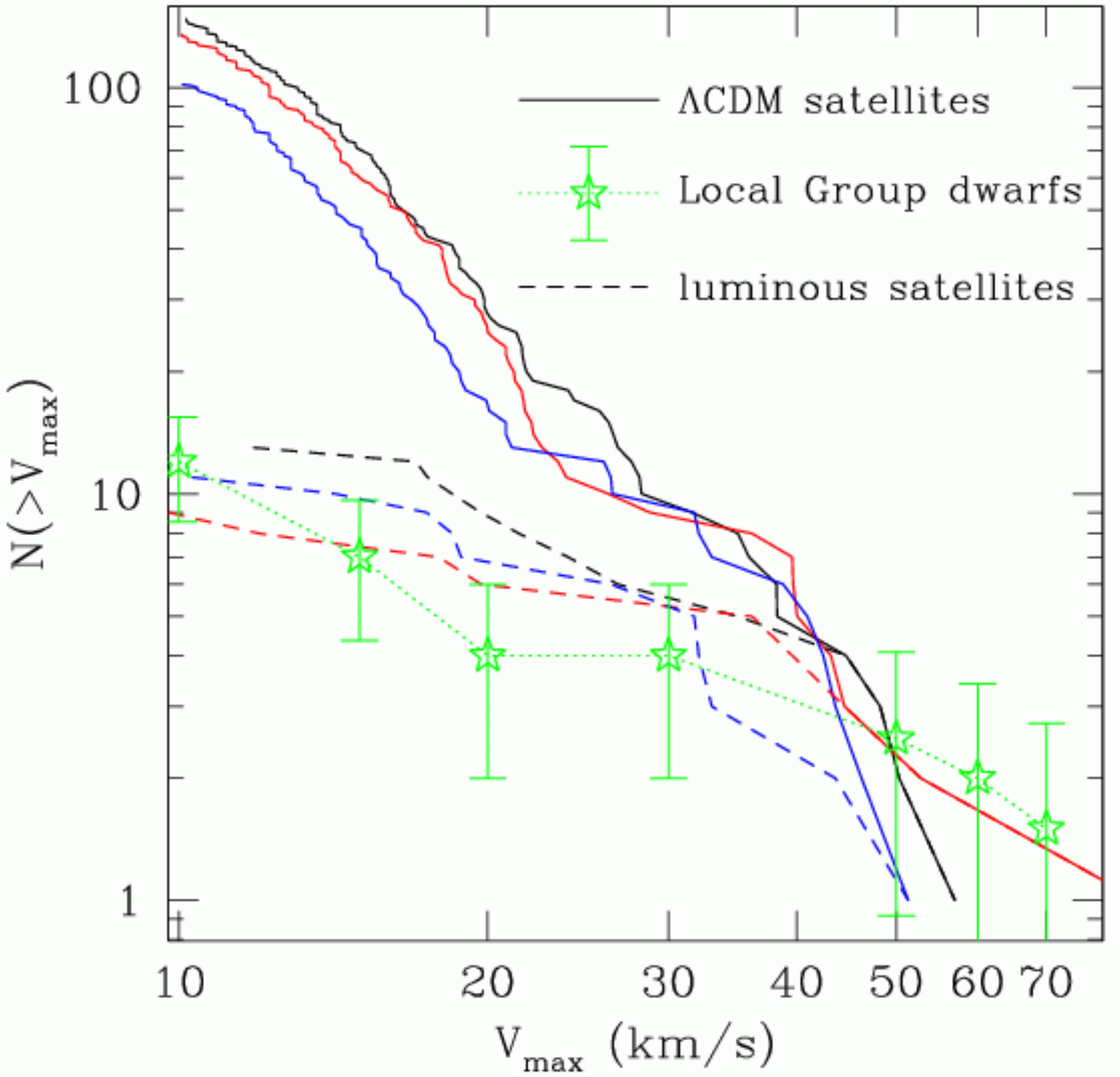

FIG. 7.— The cumulative velocity function of the dark matter satellites in the three galactic halos (*solid lines* compared to the average cumulative velocity function of dwarf galaxies around the Milky Way and Andromeda galaxies (*stars*). For the objects in simulations $V_{\rm circ}$ is the maximum circular velocity, while for the Local Group galaxies it is either the circular velocity measured from rotation curve or from the line-of-sight velocity dispersion assuming isotropic velocities. Both observed and simulated objects are

Abundance and structure of largest satellite galaxies of the Milky Way galaxy

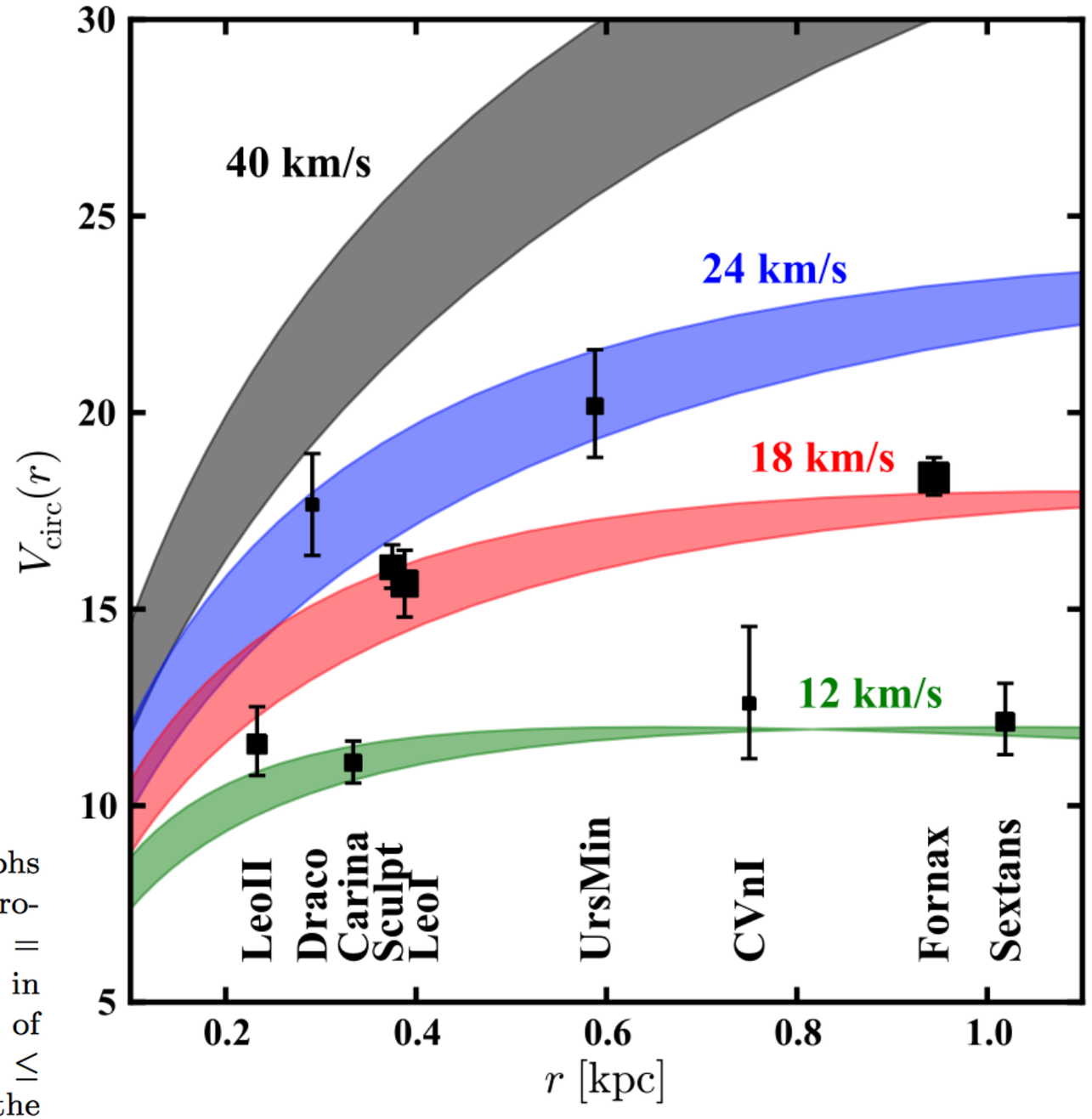

Figure 1. Observed $V_{\rm circ}$ values of the nine bright dSphs (symbols, with sizes proportional to $\log L_V$), along with rotation curves corresponding to NFW subhalos with $V_{\rm max} = (12, 18, 24, 40)\,{\rm km\,s^{-1}}$. The shading indicates the $1\,\sigma$ scatter in $r_{\rm max}$ at fixed $V_{\rm max}$ taken from the Aquarius simulations. All of the bright dSphs are consistent with subhalos having $V_{\rm max} \leq 24\,{\rm km\,s^{-1}}$, and most require $V_{\rm max} \lesssim 18\,{\rm km\,s^{-1}}$. Only Draco, the least luminous dSph in our sample, is consistent (within 2σ) with a massive CDM subhalo of $\approx 40\,{\rm km\,s^{-1}}$ at $z = 0$.

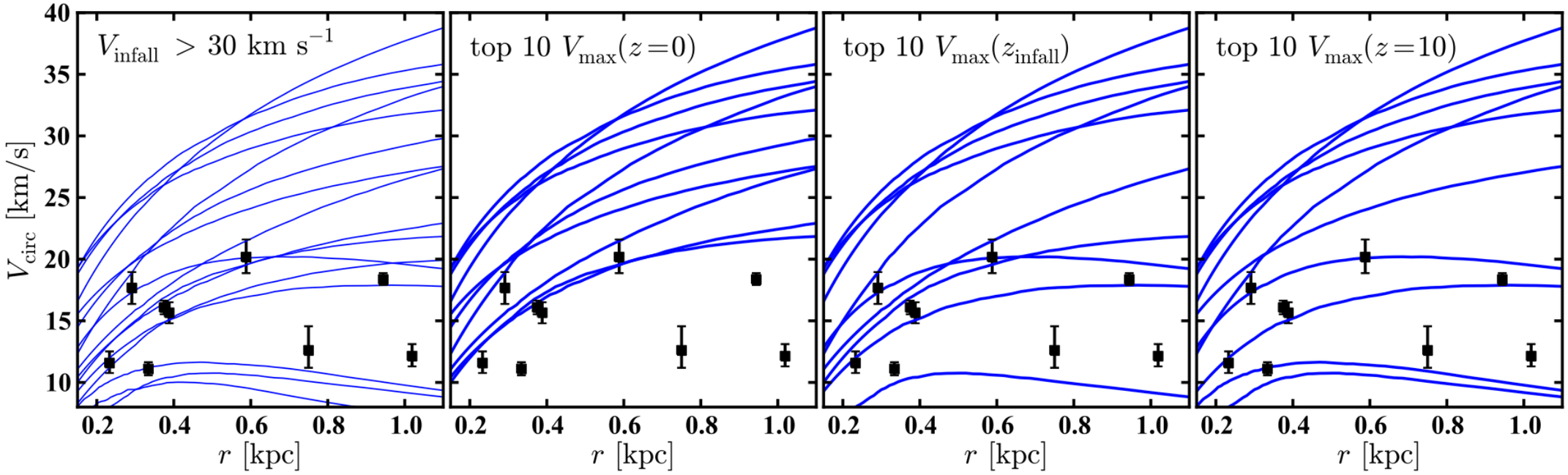

Figure 2. *Left panel:* circular velocity profiles at redshift zero for subhalos of the Aquarius B halo (top; $M_{\rm vir} = 9.5 \times 10^{11}\,M_\odot$) and E halo (bottom; $M_{\rm vir} = 1.4 \times 10^{12}\,M_\odot$) that have $V_{\rm infall} > 30\,{\rm km\,s^{-1}}$ and $V_{\rm max}(z=0) > 10\,{\rm km\,s^{-1}}$ (excluding MC candidates). Measured $V_{\rm circ}(r_{1/2})$ values for the MW dSphs are plotted as data points with error bars. Each subsequent panel shows redshift zero rotation curves for subhalos from the left panel with the ten highest values of $V_{\rm max}(z=0)$ (*second panel*), $V_{\rm infall}$ (*third panel*), or $V_{\rm max}(z=10)$ (*fourth panel*). In none of the three scenarios are the most massive subhalos dynamically consistent with the bright MW dSphs: there are always several subhalos more massive than all of the MW dSphs. (Analogous results are found for the other four halos.)

Warm dark matter

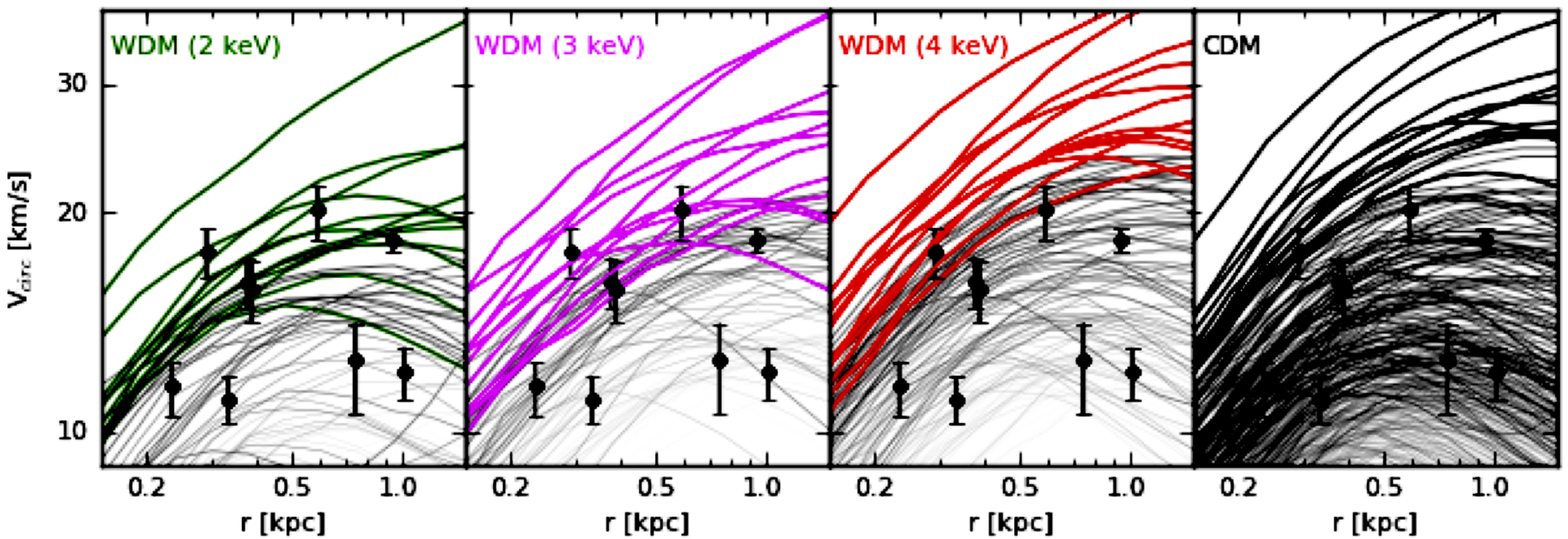

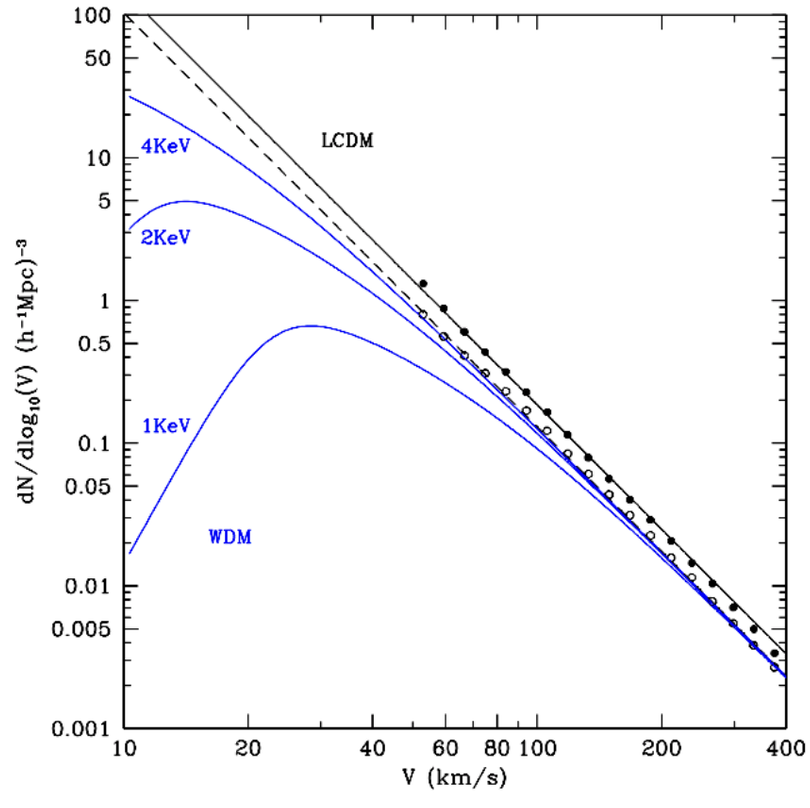

Effects of tidal stripping and ram pressure on structure of satellites: effects of baryons

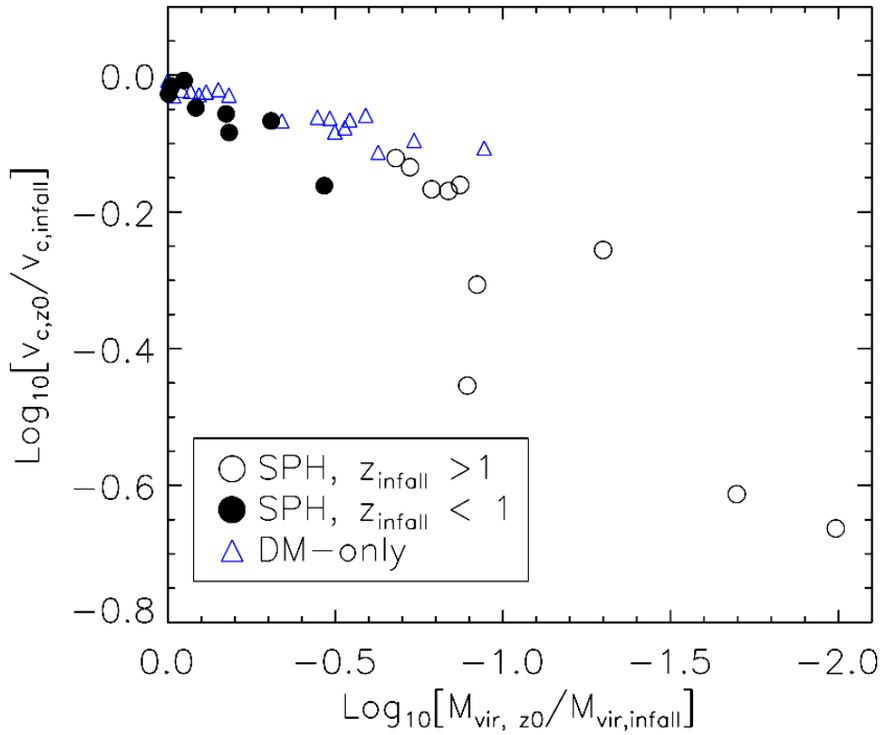

Hydro+ star formation simulations of dwarf satellites

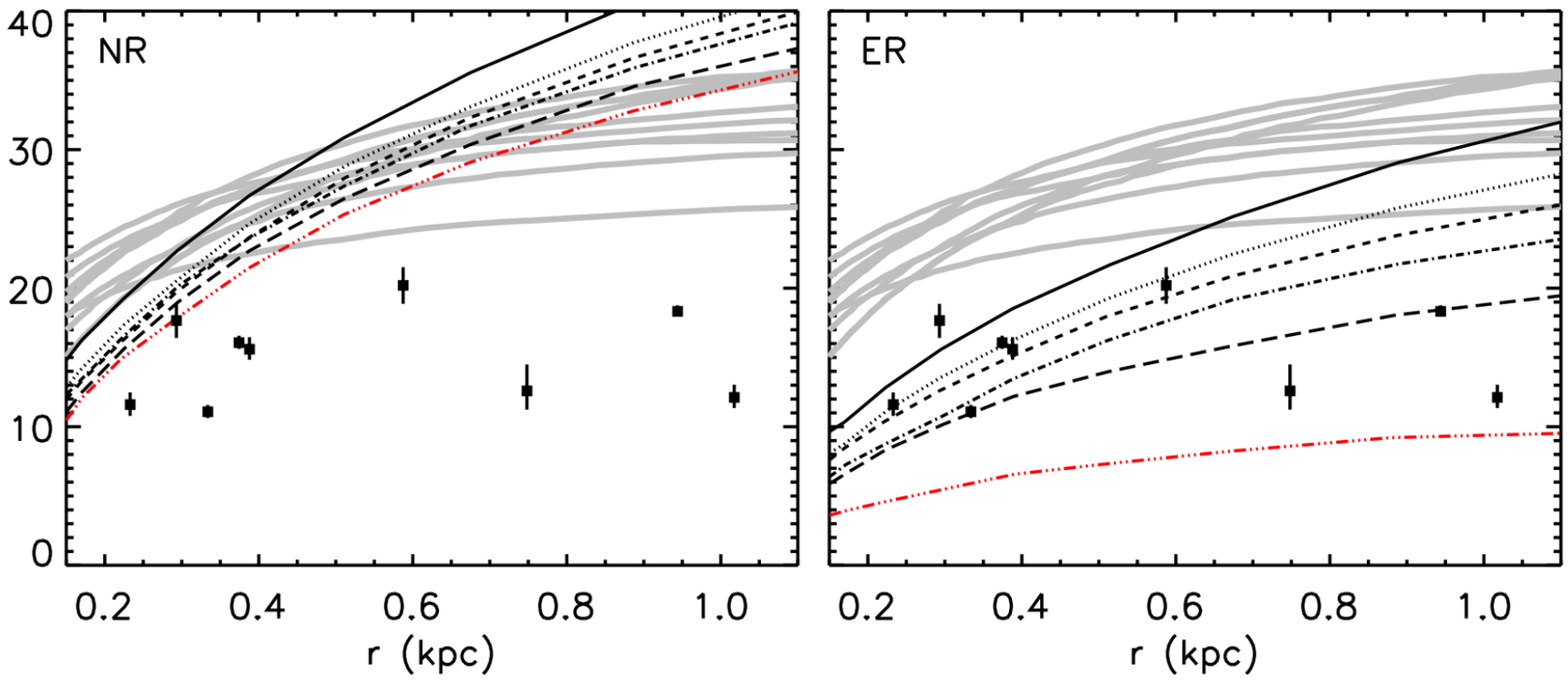

N-body simulations with a fraction of mass removed to mimic ram pressure

Comparison of our elliptical orbits to observations of the MW satellites (black squares) and the Aquarius E halo's 'massive failures' from the analysis of Boylan-Kolchin et al. (2012) (thick grey lines). Left: the circular velocity profiles of the NR case. This profile does not agree with the MW dSph population and was created to mimic the Aquarius cosmological simulations by not including the effects of baryons. Right: the circular velocity profiles of the exponential mass removal (ER) case. These profiles span a much larger range of parameter space and are in agreement with observed MW dwarfs due to their inclusion of baryonic effects. Both panels show the initial isolated profile as a solid black line. The elliptical orbits after 5 Gyr of evolution are shown from top to bottom as 150–70 kpc (dotted), 150–50 kpc (short dashed), 150–30 kpc (dot–dashed) and 120–30 kpc (long dashed). The 50 kpc circular orbit is shown as the bottom most triple dot–dashed line (red) for reference of the most dramatic orbital evolution of our simulations.